*American Journal of Sciences and Engineering Research*
*E-ISSN– 2348–703X, Volume 9, Issue 1, 2026*

# The 3-Cosmic Framework of String Theory Can Interpret Dark Matter and Dark Energy

**[1]Hsien-Jung Ho**
*10 Fl., 110-6, Jie-Shou N. Road, Changhua City, Taiwan*

**ABSTRACT:** Based on the original String theory, the universe's constitution is nine-dimensional space and one-dimensional time, and applying the "Anthropic Principle" and "Causality" deal with space and time, and the universe can be divided into triple cosmoses, i.e., a 3-cosmic framework in the universe. According to the string theory, between any two cosmoses, except for the gravitational force, there is no other fundament force implying dark matter in cosmoses other than ours. Exploring dark matter from the interior of the Earth, we found a dark planet inside the Earth but in a cosmos other than ours. Based on the data of cosmological parameters from the 1-year WMAP results to Planck Satellite 2018 results, the dark energy gradually decreased but the total matter gradually increased at the same value. This phenomenon agrees with the Big Bang theory; therefore, the current dark energy should be considered as the residual energy of the universe after the Big Bang. According to this data, the cold dark-matter density gradually increases by approximately 4.3%, implying that it exists in high-energy-density cosmoses, whereas the baryon density gradually increases by approximately 0.5%, implying that it exists in our low-energy-density cosmos. Because high-energy-density cosmoses expand rapidly, their dark matter should be subjected to a "drag" by gravity on the stars and galaxies of our cosmos, causing the expansion of our cosmos to accelerate. This study proposes that the problem of dark matter and dark energy in astrophysics should be roughly solved.

**Keywords: Keywords**: Dark matter, Dark energy, String Theory, Multiverse, Chandler wobble.

## I. INTRODUCTION

In the 1920s, Jacobus Kapteyn, the first astronomer to address the possible existence of invisible matter in the Milky Way Galaxy, used stellar velocities [Kapteyn 1922]. Subsequently, some scientists, such as Oort (1932), Zwicky (1937), Bartusiak (1988), and Stsrobinskii and Zel'dovich (1988), found unobservable matter, which was called "dark matter", amounted to more than 90 % of the mass of the entire universe. Dark matter is real and can only be detected by its gravitational influence on visible matter. In 2006, astronomers used the Chandra X-ray Observatory to observe the bullet cluster of galaxies and found a recent large collision of two galaxy clusters by separating dark matter from normal matter, which is direct evidence of the existence of dark matter [Clowe, et al. 2006]. Although almost all astronomers agree on the existence of dark matter, nothing has been gained after more than one hundred years of search.

[1] Newidea Research Center, Address: 10 fl., 110-6, Jie-Shou N. Road, Changhua City, Taiwan

 Received-10-02-2026 Accepted- 26-02-2026

In 1998, the High-Z Supernova Search Team published observations of type 1a supernova as standard candles [Riess et al. 1998], and in 1999, the Supernova Cosmology Project was launched in 1999 [Perlmutter, et al. 1999]. Two independent projects simultaneously reached the same conclusion: a completely unexpected acceleration of the universe's expansion. Their discovery led to the idea of an expansion force, dubbed "dark energy". Scientists believe that dark energy is the force that tears the universe apart, but dark matter condenses all things, and the interaction of these two forces forms the structure of the universe, as we know it today. Dark energy is a current scientific hypothesis, which acts as a sort of anti-gravity and is responsible for the present-day acceleration of the Universal expansion. However, it is neither matter nor radiation, and its physical properties are unknown.

After the Planck satellite observed the cosmic microwave background radiation, scientists deduced that the cosmological parameters of Planck 2018 results VI were taken as the current situation of the universe, that the universe is composed of approximately 4.94% of normal matter, such as planets, stars, asteroids, and gases, and the remaining 95.06% is dark matter and dark energy, of which dark matter that does not radiate or absorb light accounts for approximately 26.64%, and dark energy accounts for approximately 68.42% [Afghanis, et al. 2020].

Scientists believe that dark energy is the force that tears the universe apart, that dark matter condenses all things, and that the structure of the universe as we know it today is formed by the interaction between these two forces. As long as we can understand the assembling speed of a galaxy, we can understand dark matter and the power of dark energy tearing through the universe at the same time. Because the names of dark matter and dark energy come from astrophysics, we use the string theory of theoretical physics to address the major problems associated with astrophysics.

## II. MULTIVERSE THEORIES

### 2.1 Ten-dimensional space-time of the original string theory reveals a multiverse

To address these astrophysical questions, in the 1970s, String theory was introduced. String theory begins with the notion that point-like particles in particle physics can also be modeled as strings, which are one-dimensional objects. The characteristic length scale of strings is assumed to be on the order of Planck length, or $10^{-35}$ meters that looks just like an ordinary particle, with its mass, charge, and other properties determined by its vibrational states in different ways.

In quantum field theory, when a string moving in the framework of time and space is so complex that three-dimensional space cannot accommodate its motion orbit, up to nine-dimensional space must be available to accommodate the motion. Thus, all objects are considered a nine-dimensional space of the string. The string theory describes all fundamental forces and forms of matter and potentially provides a unified description of gravity and particle physics. Based on the original string theory, the universe's constitution is nine-dimensional space and one-dimensional time, which is interpreted as the product of ordinary 4-dimensional spacetime, and 6-extra-dimensional space, but 6-extra-dimensional spaces are yet unobserved [Scherk & Schwarz 1975].

Many mathematicians and physicists have attempted to break (compactify) the constitution of a ten-dimensional space-time model through spontaneous symmetry breaking, to a four-dimensional one as our known world and 6-extra-dimensional space, which is compacted to be a tiny space, called Calabi-Yau space, as Planck space. No proposed method meets perfection because there is no exact boundary condition to fit the real universe and work out a theoretically solid basic geometry.

The nine-dimensional space should be symmetrical without considering compaction, i.e., it should be symmetrical with the same weight for each dimension of space. Therefore, the universe should still exist in an equal weight of nine-dimensional space plus one-dimensional time. Thus, the string theory of the cosmic framework should still be able to maintain a complete ten-dimensional spacetime.

In multidimensional string theory, gravity is the only force of nature that has an effect across all dimensions. This explains the relative weakness of gravity compared with other fundamental forces of nature (e.g., electromagnetic force) that cannot cross into extra dimensions. In that case, dark matter could exist in extra-

dimensional space, where it only interacts with matter in our space through gravity. Dark matter can aggregate in the same way as ordinary matter, forming extra-dimensional galaxies [Siegfried 1999].

Dvali (2004) proposed that the extra dimensions of space do not curl up (not compactify) into a minimum, but rather are infinite in size and uncurved, just like our ordinary three-dimensional view. In the character of string theory, he rethinks the "extra dimensions" problem, that is, gravity can roam to any additional dimension of space. This theory predicts that the universe has extra dimensions into which gravity, unlike ordinary matter, can escape. This leakage would warp the spacetime continuum and accelerate cosmic expansion. Thus, the extra dimensions do not need to be small and compact but may be large extra dimensions, i.e., outside our ordinary three-dimensional space, there are the same six extra dimensions of other space usually in the universe.

**2.2. Some cosmologists accept this multiverse concept at present**

In the 1950s, Hugh Everett devised the "many-worlds interpretation" (MWI) of quantum mechanics. The core of the idea was to interpret in the quantum world that an elementary particle, or a collection of such particles, can exist in a superposition of two or more possible states of being [Everett 1957]. An electron, for example, can be in a superposition of different spin locations, velocities, and orientations. However, scientists obtain a definite result whenever they measure one of these properties with precision just an element of the superposition, not a combination of them. No macroscopic objects are observed in the superposition. The many-world interpretation is a multiverse theory (Byrne 2008).

In the 1980s, American physicist Alan Guth, who studied cosmology, proposed inflation theory, which explained that the universe expanded at a very rapid rate of geometric progression, and the volume expanded by a hundred thousand times in an instant after the Big Bang. When the expansion stops, it will not stop completely at the same time. It will stop in some places, and those places will become the universe. In other places, the expansion will continue. Later, more small universes will form, and countless small universes may form. We now call them multiverses, and this process is called permanent expansion; therefore, there are innumerable universes, not just one universe [Guth 1982]. A multiverse is a hypothetical group of multiple universes.

In the 1980s, Leonard Susskind said that it was the result of string theory, which was used as a tool or framework to describe cosmic phenomena [Susskind 2006]. MWI is a theory of multiple universes. In this case, scientists can produce the only explanation: these elementary particles do not exist only in our cosmos; they may also fly around other cosmoses that are not ours. This means that there may be multiple cosmoses, called multiverse, in space, but only subtle differences exist between them, so there are still cosmoses about which we do not know. An important aspect is the extension of physical theories within a multiverse framework. The dominant expectation so far for the theory of quantum gravity (QG) has been the "reductionist" hope that relies on QG producing a unique solution that resembles the general features of our universe, but scientists have failed to achieve this goal. The three different and important theories: quantum mechanics, string theory, and inflation, predict the existence of the multiverse, which scientists believe is hardly coincidental. The existence of the multiverse can be expected from the underlying fundamental theory.

David Deutsch is a leading figure in multiverse theoretical physics. He believes that this multiverse theory is the only explanation for the strange phenomenon in quantum mechanics because it is based on rigorous mathematical equations and many experimental results [Deutsch 2010]. Although more than 50 years have elapsed since the first discussion of the "many worlds" by Everett, no new step has been taken to establish the foundations and ontology of the multiverse and of this new field in physics.

**2.3 The map of microwave background radiation fluctuations may provide hard evidence of another cosmos**

In June 2001, NASA launched Wilkinson Microwave Anisotropy Probe (WMAP), which was designed to detect residual cosmic radiation heat in the universe after the Big Bang and to draw a full map of microwave background radiation fluctuations throughout the universe. In 2009, the European Space Agency's partnership with NASA launched the Plank Satellite, which can detect tiny temperature fluctuations in this radiation. Then, a fluctuation map of cosmic microwave background radiation was drawn with greater accuracy.

In general, scientists tend to think that the radiation is evenly distributed, but the full map shows a different fact – there is a powerful center in the sky in the southern half of the map and a seemingly hole-like "cold spot" where galaxies are accelerating away that cannot be explained by existing physics knowledge [Rudnick, et al.

2007].

Some scientists have proposed multiverse perspectives to explain the cold spot from this anomaly. Scholars have predicted that string theory does not predict a unique universe; on the contrary, it does predict a multiverse [Mersini-Houghton 2008]. In 2005, scientists predicted the existence of anomalies in radiation existed that could only have been caused by gravitational pulling on our cosmos from others as it formed during the Big Bang [Woit 2013]. The "cold spot" in the southern half of the map of the universe may be the first "hard evidence" of another cosmos than ours that exist has been found by scientists [Leake 2013].

String theory states that the three-cosmic framework of the universe has characteristics in which each cosmos describes a world of general matter, whereas the others describe other worlds that we know nothing about. Among any other cosmoses, there are no basic interactive forces of nature except gravity; in other words, theoretic gravitons in the field of gravity can penetrate all three cosmoses; however, light (electromagnetic wave) cannot, meaning that dark matter may exist in cosmoses other than ours, i.e., the space of the universe is multiverse.

**2.4 Based on theories figure out a 3-cosmic framework in the universe**

The ten-dimensional spacetime of string theory is considered to exist universally without compacting the nine-dimensional space of the universe. According to "Causality", an effect cannot occur before its cause, which means that time has one direction and cannot be divided into different parts. Thus, one-dimensional time is taken as the standard for the order of events in the universe. According to the "Anthropic Principle", we live in a universe set up to allow for our existence. This means that 3-dimensional space and 1-dimensional time, called 4-dimensional spacetime, are taken together as one cosmos as our living world. Therefore, the 9-dimensional space can be divided into three portions, each with a common standard time. This means there is a 3-cosmic framework in the universe, called triple cosmoses; in other words, the universe contains three cosmoses, which are located in the same nine-dimensional space.

According to string theory, a 3-cosmic framework of the universes in which our cosmos describes the world of general matter as we know it, while others describe another world, which we know nothing about, is a three-cosmic framework. Among any other cosmoses, there are no fundamental forces of nature except gravity; in other words, the graviton in the field of gravity can penetrate all three cosmoses; however, light (electromagnetic wave) cannot that means among the cosmoses cannot be observed directly with each other.

According to this 3-cosmic framework of the universe, there are triple cosmoses in the whole space, namely 1st cosmos, 2nd cosmos and 3rd cosmos, where $U_1$, $U_2$, and $U_3$ are used instead. In the 3-cosmic framework of the universe, fundament forces do not exist between any two cosmoses except for the gravitational force, i.e., cosmoses cannot interact directly with each other, which is characteristic of dark matter. Therefore, dark matter, which will be discovered through gravity, should exist in cosmoses other than ours.

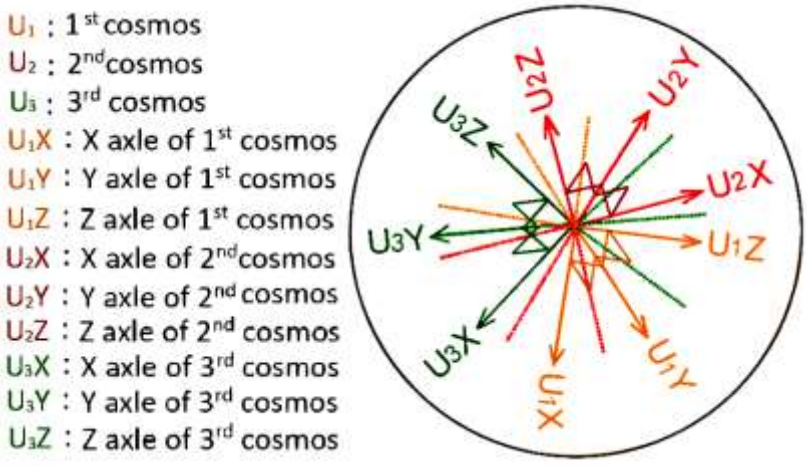


*Figure1. Schematic representation of nine-dimensional space in 3-cosmic framework of the universe.*

As shown in Figure 1, all the 3 cosmoses ($U_1$, $U_2$, and $U_3$) exist, but none of the fundamental forces can affect each other except gravity; for example, if $U_1$ is our cosmos, we cannot observe $U_2$ and $U_3$. The 3 axles (X, Y, and

Z) are all perpendicular to each other in each cosmos. In the diagram, the center of the circle is assumed to be a point P, which has 9 coordinates: $U_1Xp$, $U_1Yp$, $U_1Zp$, $U_2Xp$, $U_2Yp$, $U_2Zp$, $U_3Xp$, $U_3Yp$, and $U_3Zp$ in the universe [Ho, 2022]. Assuming a star at position P, which appears in our cosmos, the other cosmoses cannot observe the star; its coordinates are only denoted by Xp, Yp and Zp, respectively.

## III. METHODS

### 3.1 Exploring dark matter starts from the Earth

Based on the original string theory and the 3-cosmic framework of the universe, we can investigate dark matter in cosmoses other than our own. The best method for exploring dark matter is to start from the Earth, where we live. In the current Earth model utilized in seismological investigations, such as body-wave travel times, surface-wave dispersion, and free oscillation periods for researching the Earth's chemical composition and density distribution, some Earth data can be analyzed. The portions of the crust and upper mantle were analyzed with satisfactory accuracy. However, regarding the lower mantle and core, several questions remain to be answered. Two convections circulate individually below the crust to the lower mantle and in the outer core itself. The mantle and core are not in chemical equilibrium, and the fine structure of the core-mantle boundary (CMB) is not well understood. Although some hypotheses, such as the existence of a D″ layer in the lower mantle and iron combined with oxygen as the primary alloying constituent of the outer core, have been proposed, and many advances in this research have been made, there are also some discrepancies in the interior of the Earth [Morelli & Dziewonski 1987]. Furthermore, no conclusive evidence exists that the inner core is in thermos-dynamic equilibrium with the outer core.

The main problem is the lack of phase-equilibrium data for plausible core compositions under the appropriate conditions, in addition to the fact that seismological observations do not yet offer a decisive constraint on the difference in composition between the inner and outer core [Jeanloz 1990]. A different perspective of the deep interior of the Earth should be taken to analyze the Earth's constitution, composition, temperature, and pressure, and a revolution in its chemical composition should be developed to investigate the outer core.

### 3.2 Arguments at the core-mantle boundary

The constitution of the deep interior of the Earth is uncertain, and there are some difficulties. The Preliminary Reference Earth Model (PREM) [Dziewonski & Anderson 1981] was taken as the current Earth model in this paper to conduct further investigations. There are arguments in the topic of CMB as follows:

1. Ramsey (1948) and Lyttleton (1973) challenged the concept of an iron core, stating that the CMB is the boundary of Ramsey's phase change, not the interface between silicates and the iron core.
2. Knopoff (1965) showed that the bulk modulus remains constant so that the density distribution at the CMB should be continuous.
3. Buchbinder (1968) studied the variation in the reflection amplitudes of seismic waves and found that they show a phase change at the CMB.

From items 1, 2, and 3, it can be initially identified that the mantle and core materials mix with each other, and the density distribution between the lower mantle and the outer core should be consistent to solve some geophysics problems. The main components of the outer core should be considered as the same ingredients of molten rock and mineral silicates, which are chemically consistent with the lowermost mantle's ingredients.

The isotopic composition of lavas associated with mantle plumes has previously been interpreted in the light of core–mantle interaction, suggesting that mantle plumes may transport core material to the Earth's surface (Mundl-Petermeier, et al. 2020; Rizo, et al. 2019; Horton, et al. 2023; Mundl, et al. 2017). The combined ruthenium and wolfram isotope systematics of Hawaiian basalts are best explained by simple core entrainment and core-derived oxide mineral addition at the CMB [Messling, et al. 2025]. The main components of the outer core are molten rock and/or mineral silicates, which are chemically consistent with the lowermost mantle, and some matter, such as the metal platinum [Hecht 1995] and osmium-187 [Walker, et al. 1995], are brought from the core all the way to the surface of the Earth that flows between the F layer and the Earth's crust, causing the more than 10 km relief of the CMB [Morelli & Dziewonski 1987].

### 3.3 CMB topography revealed that both sides were made of the same materials

A sufficient quantity of high-quality digital data from two global networks: a network for very long-term seismology [Agnew, et al. 1976] and a seismic research observatory [Peterson, et al. 1976], which began operation in the mid-1970s and developed over four decades, provided the framework of formal analysis. The availability of computers made the handling of immense amounts of data feasible and the large-scale calculations necessary for three-dimensional problems. Geophysicists recorded more than 15,000 times the magnitude 4.5$^{th}$-class earthquake data on Earth, input a seismic laboratory computer, drawn a three-dimensional topographical map of the Earth's interior, and produced computer tomography X-ray photographs, producing the CMB topography, which is found in the boundary of the solid mantle and the liquid outer core. Maps of the CMB topography have been derived on the basis of seismological inversions of long-wave travel times to construct three-dimensional maps with the magnitude of amplitudes from ±3 km up to ±6 km (largest relief 12 km) and with 3000 ~ 6000 km scale lengths [Doornbos & Hilton 1989; Forte & Peltier 1991; Neuberg & Wahr 1991; Rodgers & Wahr 1993; Obayashi & Fukao 1997; Boschi & Dziewonski 1999, 2000; Garcia & Souriau 2000; Sze & van der Hils 2003; Yoshida 2008; Soldati, et al. 2013; Soldati, et al. 2014].

In three-dimensional maps of the Earth's interior, the topography of the CMB differs from that predicted by hydrostatic equilibrium theory, which contains information important to geodynamic processes and geomagnetic secular variation. The CMB topography is likely due to convection in the overlying mantle [Young & Lay 1987]. Ruff and Anderson (1980) argued that dynamo action in the core was maintained by differential heating of the core by the mantle, and some agreements with them were probably determined by core processes [Bloxham & Jackson 1990]. The depressed regions of the topography are dynamically supported by the downwelling of cool mantle material [Lay 1989], indicating that the relief is dynamically supported and provides coupling between the solid mantle and the fluid core. Scientists suggest that the topography associated with subduction slabs has additional effects, which may have a mechanical rather than thermal effect on the flow [Gubbins & Richards 1986].

The Gravity Recovery and Climate Experiment (GRACE) satellites and Satellite Laser Ranging (SLR) were used to explore the Earth's gravity field between 2003 and 2015 to understand its deep interior. As the gravity signals originate deep within the Earth, these data may provide innovative information on mass redistributions near the core-mantle boundary. The results suggest that it may reflect rapid mass redistributions linked to mineral phase transition occurring in a thermally varied area at the base of deep mantle plumes, potentially causing dynamic changes in the core-mantle boundary's shape [Gouranton, et al. 2025].

In terms of geodynamic processes, only the vertical interactions of the material and the temperature between the lowermost mantle and the outer core are the main causes. To maintain the 10 km of relief, the density difference between the liquid and solid states at the CMB must be very small; thus, the density of the materials between both sides at the CMB must be similar or equal, i.e., the same materials between the solid mantle and liquid core change state with each other at the CMB.

### 3.4 Heat flow of core leaks into the mantle

Geophysicist Morgan (1971) proposed the hypothesis of mantle plumes, which are generated from thermal boundary layers and have been invoked for decades to explain the formation of hotspots and flood basalt provinces on Earth. In this hypothesis, convection in the mantle transports heat from the core to the Earth's surface in thermal diapirs. Two largely independent convective processes occur in the mantle. 1. *Mantle plumes* carry heat upward in narrow, rising columns driven by heat exchange across the core-mantle boundary to the crust. 2. The broad convective flow associated with *plate tectonics* is primarily driven by the sinking of the cold plates of the lithosphere back into the mantle [Morgan 1972].

Mantle plumes are hot rock tubes rising from Earth's core, many of which lie beneath known volcanic hot spots at Earth's surface. The thermal plumes are fatter than expected, meaning that they carry more heat away from the Earth's core, indicating that plumes are important for cooling the Earth's surface [Hand 2015].

The heat loss from the Earth's surface is greater than that from the Sun. If the core did not continue to release heat, the Earth would have cooled off and become a dead rocky globe, such as Mars or the Moon. Releasing

heat is by nuclear energy from the much slower decays of radioactive elements, such as $^{238}U$, $^{235}U$, $^{232}Th$, and $^{40}K$ [Van Schmus 1995]. However, the radiogenic heating generated in the core turns iron into a convecting geo-dynamo that maintains a strong magnetic field, shielding the planet from the solar wind. This heat leaks out of the core into the mantle, causing convection in the rock or molten rock that moves the crustal plates and fuels the volcanoes.

In 1997, seismic tomography was used to image submerging tectonic slabs penetrating from the surface all the way to the core-mantle boundary [Kerr 1997]. The hotspot's volcanic activity continues to produce basalt lava, which forms the Hawaiian Islands and Iceland. Norwegian scientists discovered that basalt eruptions in the Hawaiian Islands and Iceland varied significantly over time [Mjelde & Faleide 2009]. As these two hotspots are located on opposite sides of the Earth, Mjelde and colleagues suggested that the co-pulsations represent a global hotspot phenomenon that appears to represent changes in heat from the Earth's core [Mjelde, Wessel & Müller 2010]. Knittle and Jeanloz (1991) proposed that the core generates a significant amount of energy driving the mantle convection. When checking the temperature of the Earth's interior, the hottest point is the center of the Earth at approximately 7000°C [Kubala & Mahan 1996], in the inner-core boundary (ICB) at over 6000°C [Condie 1997], and in the CMB about 4180 ±150°K [Fiquet, et al. 2010] (Figure 2).

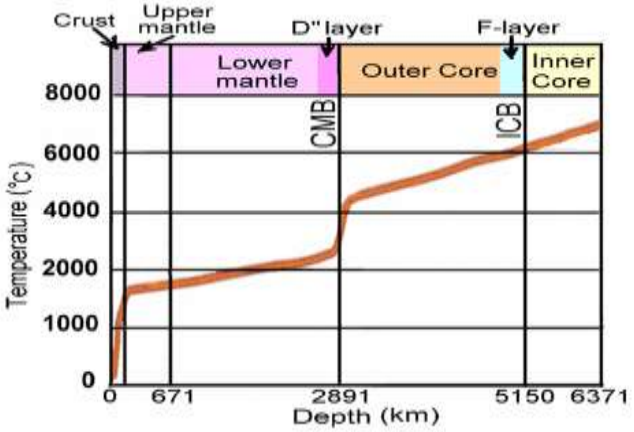


*Figure 2. The temperature profile of the Earth's interior*

The abundant heat flow from the fluid core leaks into the mantle. In higher resolution models, the internal effects of the liquid outer core cause some heterogeneities to extend upward from the CMB into the mantle in a manner suggestive of a rising thermal plume structure [Young & Lay 1987]. Thermal plumes from the Earth's core are rising tubes of hot or molten rock that carry more heat away [Hand 2015].

**3.5 The great convection cell spanning the crust through the CMB to the F-layer is shown.**

On this basis, a large quantity of magma heated at extreme temperatures in the core solidifies into rock, producing solidification heat at the CMB. A few quantities of magma absorbing this heat do not solidify but mix with masses of rock as honeycombed blobs of rock and bring some materials, including magma, osmium-187, $^{3}He$, and a little metal, platinum, upward the mantle to pour out at cracks in the mid-ocean ridge to form new ocean floors or in the continent to form great rifts, which works as a secular cooling of the Earth. The downward masses of the slab in the cold regions of the low mantle produce CMB depressions into the core, and both the cold region in the mantle and a CMB depression produce downwelling flows into the core [Bloxham & Jackson 1990].

The depressed regions of the topography on the CMB are dynamically supported by the downwelling of cool mantle materials, which then flows through the CMB into a liquid core, probably determined by the core [Lay 1989]. The outer core materials absorb the abundant heat flow and form an upward convection thermal plume. The energy and buoyancy sources in the core are still not well understood, but we attempt to explain this phenomenon from the perspective of a convection cell. The downward masses of the slab absorb the heat of fusion, diminishing the heat energy at the CMB and melting in the core, where the viscosity is so high that a large quantity of molten rock cannot diffuse but remains as a whole. Thus, molten rock components are rarely involved in chemical reactions.

According to the mechanics, although the velocity of the downward migrating flow is low, the mass of the slab plate from the crust to the CMB is so large that its downward momentum has a large quantity. In the liquid outer core, there is no rigid body with sufficient mass to counteract the downward momentum; thus, the molten rock sinks into the lowermost fluid core. The great downward momentum is counteracted merely by the solid inner core, from which Jeanloz and Wenk (1988) obtained possible evidence of low-degree convention like it in the mantle of the inner core from an enigmatic observation.

Seismological studies have indicated that the Earth's inner core is anisotropic for P waves and has low S-wave velocity and high seismic attenuation. The presence of a liquid volume fraction of 3%~10% in the form of oblate spheroidal inclusions aligned in the equatorial plane between iron crystals is sufficient to explain the seismic phenomena. The liquid could arise from the presence a "mushy zone" of dendrites or a mixture of elements other than iron in liquid form under inner-core conditions [Singh, Taylo & Montagner 2000]. Bergman (2003) and Shimizu, et al. (2005) suggested that a thin, mushy layer develops underneath the ICB, while the materials of the outer core solidify onto the inner core. Therefore, the inner core should not be a rigid spheroid. At the ICB, the momentum from the downward molten rock is transmitted through the inner core of the Earth's center and probably to the opposite side of the CMB. This phenomenon can be inspected using a three-dimensional topographic map of the CMB on Earth (Figure 3) [Morelli & Dziewonski 1987].

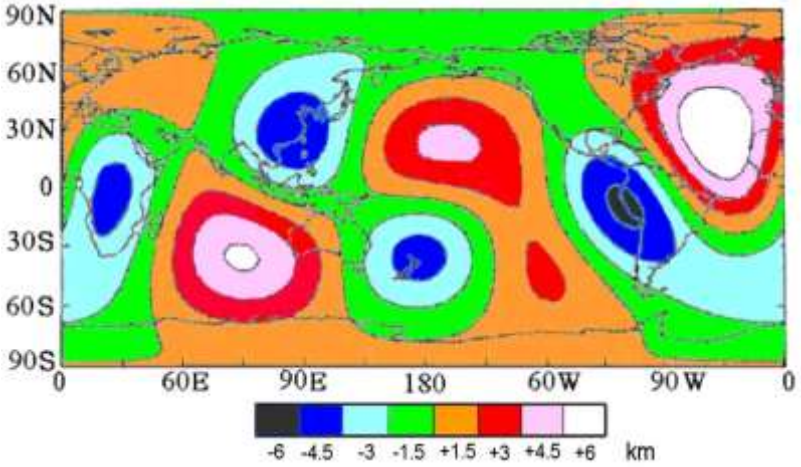


*Figure 3. The topography of the CMB obtained by inversion of the combined PcP and PKPBC dataset.*

It is magma that sinks toward the ICB, and its kinetic energy becomes pressure and spreads into the earth's inner core. It pushes and shoves the opposite side of the ICB, even forming a rough CMB. As shown in Figure 3, the CMB is concave in New Zealand but protrudes in the North Atlantic Ocean. The CMB under the west coast of South America is concave but protrudes in the region of Western Australia and near the Indian Ocean. The CMB under South Africa is concave but also protrudes in the North Pacific Ocean. There is a significant suggestion that the same materials, mainly silicates, of the rocky mantle and the liquid outer core change states with each other at the CMB to relieve the CMB topography over 10 km. A reasonable explanation may be that the plate's migrating or molten rock sinks downward, and a magma or thermal plume rises upward in the great convection cell spanning the crust through the outer core's F-layer.

**3.6 Arguments at the inner core boundary**

The seismic structure of the Earth's inner core is highly complex, with strong anisotropy and regional variations. However, few seismic waves are sensitive to the inner core, and fundamental questions regarding the origin of the observed seismic features remain unanswered [Waszek & Deuss 2015a]. The inner core solidifies from the outer core; however, the details of this process remain largely unclear [Pejić & Tkalčić 2016].

Seismologists have yet to answer some fundamental questions concerning the core, including the low-velocity gradient region at the lowermost outer core. Numerous seismological studies have proposed that the region just above the ICB is distinct from the outer core. The layer approximately 400 km above the ICB was originally termed the F-layer and was characterized by a strong low-velocity zone [Jeffreys 1939]. After studying the velocity and amplitude in the core, scientists inferred that the highly separated solutions of the F-layer are around the ICB

[Bolt 1972; Qamar 1973]. Most observations indicate that the F-layer is global and surrounds the entire inner core (Souriau & Poupinet 1991; Zou, Koper & Cormier 2008; Cormier, Attanayake & He 2011).

Ray theory has been used to interpret evidence of a reduced seismic wave velocity gradient to near 0 in the F-layer of the outer core [Rial & Cormier1980; Cormier 1981]. Later Earth models were constructed with more accurate travel-time data but were defined as regions of increased velocity. Among the velocity models at the base of the outer core reported by different studies (e.g.: Qamar 1973; Choy & Cormier 1983; Souriau & Poupinet 1991; Song & Helmberger 1995; Kennett, et al. 1995; Yu, et al. 2005), the main difference is the velocity structure and its gradient at the bottom 400 km of the outer core. According to Earth's models, such as: PREM2 [Song & Helmberger 1995], AK135 [Kennett, et al. 1995] and Jeffreys-Bullen model [Jeffreys 1939], a low-velocity gradient region at the lowermost outer core is denoted by Bullen and bolt (1986). In PREM, the velocity increased with a nearly constant gradient around $0.6\times10^{-3}$ $s^{-1}$. In PREM2 and AK135, the velocity gradient decreases from about $0.6\times10^{-3}$ $s^{-1}$ at 400 km above the ICB to nearly zero at the ICB, and the velocity profile with depth was flatter than that in PREM (Figure 4). Therefore, 400 km above the ICB was chosen as the minimum "pinning depth", at which the models were evaluated and constrained to agree with the PREM in terms of the value and gradient.

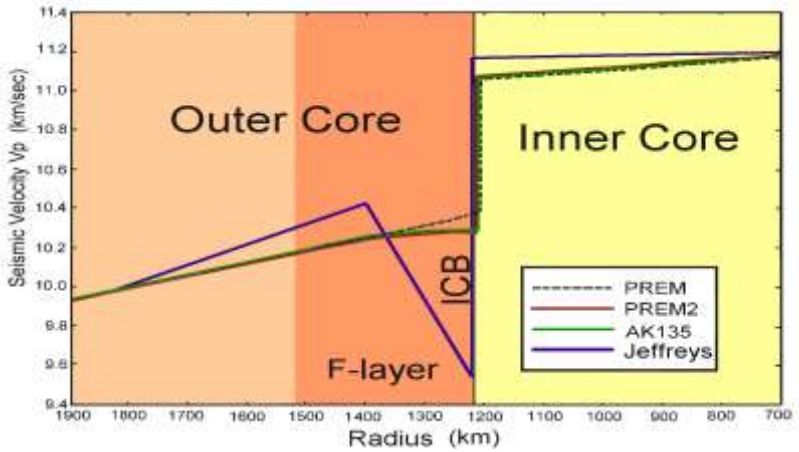


*Figure 4. Variation chart of seismic wave velocity in the Flayer: Vp low-velocity gradient and sharp-velocity discontinuity at the ICB indicate their different components.*

While the seismic wave entered the F-layer, a sharp velocity discontinuity appeared at the ICB, the velocity jumped 0.78 km/sec, and a low velocity gradient appeared at the fluid core base, indicating slightly different components. The most robust pointer to the viscosity at the bottom of the outer core may still be the reduced P-velocity gradient, which is difficult to explain without appealing to the existence of a chemical boundary layer [Song & Helmberger 1995; Kennett, et al. 1995]. These models imply that the density near the base of the outer core increases too quickly to be explained solely by compression and that some sort of change in chemistry and phase may occur.

Experiments [Sumita & Olson 1999; Sumita & Olson 2002] and numerical simulations [Aubert, at al. 2008] have shown that outer-core convection can be used to transmit temperature anomalies generated by strongly heterogeneous CMB heat flux from the CMB to the ICB. As the Earth cooled and dissipated its internal heat toward the surface through mantle convection, the geographical coincidence of the ICB and CMB anomalies suggests strong thermal coupling of the mantle and the core, indicating a convection cell across the CMB. Instead of the well-known D" layer, the F-layer should have some functions, such as thermal and chemical equilibrium.

**3.7 Density jumps at the ICB**

Regional differences in *PKIKP-PKiKP* travel times and amplitude ratio data may originate from the F-layer. Bolt and Qamar (1970) proposed the amplitude ratio (*PKiKP/PcP*) technique and estimated a maximum density jump of 1.8 g/cm$^3$ at the ICB. Bolt (1972) clearly observed both low-angle and steep incident reflection of PKiKP of approximately 1 second period at the ICB. The mean amplitude ratio *PKiKP/PcP* proposes a density jump Δρ of 1.4 g/cm$^3$. Souriau and Souriau (1989) used the amplitude ratio *PKiKP/PcP* at short distances to constrain the

density jump at the ICB to be in the range of 1.35 ~ 1.66 g/cm$^3$ based on array data. Shearer and Masters (1990) used "non-observations" of *PKiKP* on the observed amplitude of this phase, leading to upper bounds $\Delta\rho$=1.8 g/cm$^3$ at the ICB on the corresponding *PKiKP/PcP* amplitude ratios. PKiKP has been used to calculate the density jump $\Delta\rho$ across the ICB, and this has remained a topic of debate until now [Waszek & Deuss 2015b]. At the ICB, a density jump of 0.68 g/cm$^3$ in the PREM was too small to be compared with previous data.

As previously stated, the density difference between the outer and inner core must be substantial. Jeanloz and Ahrens (1980) conducted shock wave experiments and found that the density of FeO was 10.14 g/cm$^3$ when reduced to the core temperature and 250 GPA pressure, and under the same conditions, the density of Fe was 12.62 g/cm$^3$ [McQueen, et al. 1970] when FeO became Fe. The difference between the two is 2.48 g/cm$^3$, which is higher than all other evaluated values.

The density jump between the lighter liquid outer core and the solid inner core seems to be too large to represent a simple volume change during condensing as the same major components change from a liquid state Fe to a solid-state Fe. The composition of the outer core is not likely to be the same as that of the inner core because a liquid in equilibrium with a solid phase in a multicomponent system does not have the same composition as a solid [Hall & Murthy 1972]. The major component of the outer core was mineral silicates, but iron was present in the solid inner core.

Based on the free oscillation periods, Derr (1969) inferred an earth model DI-11 by least-squares inversion with an inner core average shear velocity of 2.18 km/sec and a density jump of 2.0 g/cm$^3$ at its boundary that satisfied the known mass and moment of inertia. In this study, we used the largest density jump of 2.0 g/cm$^3$ suggested by Derr to research the new earth model.

**3.8 Examining the chemical composition of the core**

To confirm the favorable constitution of the Earth, the chemical composition of its core must be further investigated. The composition of the Earth's core is one of the most important and elusive geophysical mysteries. There is no perfect explanation for the chemical equilibrium between the core and the mantle, and the inner core and outer core are not in thermodynamic equilibrium [Jeanloz 1990].

The lower mantle's physical and chemical properties are poorly understood, and the coupling mechanisms between the mantle and the core are poorly understood at all timescales. However, the CMB sets boundary conditions for processes occurring within the core, a well-known fact. The variations in topography and lateral temperature in the lowermost mantle may have an indistinguishable effect on the magnetic field [Bloxham & Gubbins 1987]. Secular variations with periods shorter than a million years but longer than several years almost certainly originate from processes operating in the outer core; unfortunately, there is no consensus as to what those processes are [McFadden & Merrill 1995].

Topographic models represent instantaneous, low-resolution images of a convicting system in three-dimensional maps. Detailed knowledge of mineral and rock properties that are poorly understood at present is required. A complex set of constraints on the possible modes of convection in the Earth's interior that have not yet been worked out; this will require numerical modeling of convection in three dimensions. Thus, the interpretation of the geographical information from seismology data in terms of geodynamic processes is a matter of considerable complexity. The topography of the CMB can only be sustained by dynamic processes, and these processes must be critically understood [Woodhouse & Dziewonski 1989].

The fine structure of the CMB is not well known, but it contains important information about the mantle's geodynamic processes or the magnetic fields generated in the outer core [Anzellini et al. 2013]. Approaching the CMB problem, Creager and Jordan (1986) studied the travel time anomalies of *PKiKP* and $PKP_{AB}$ and corrected the mantle structure in a region near the CMB. They considered some hypotheses regarding the source of anomalies that are perturbations in the CMB topography. Based on the great convection cell, a relief of the core of more than 10 km, as provided by the three-dimensional maps, may be accepted.

As previously stated, the main components of the outer core, i.e., mineral silicates, were similar to those of the lower mantle. Based on mineralogy, the main mineral of the mantle is pyrolite, a silicate-containing compound, and the main components of the outer core are pyrolite, but only in liquid form. Under the same conditions, the

higher the temperature at which common minerals are produced, the lower the polymerization rate, and vice versa. The closer the crystal minerals of the mantle were exposed to temperature and pressure, the greater the polymerization losses of the crystalline minerals. The mineral compounds' bonding forces are then destroyed, and crystallization gradually diminishes.

In the F-layer of the deeper core, at temperatures above 6000°C [Condie 1997], polymerization may cease completely, the bonding power of ions is mostly lost, and only the electronic bonding force exists. All ions and molecules may become unbounded. Therefore, the molten rock or magma becomes a mixture of oxides, such as: FeO, MgO, NiO, $SiO_2$, $Fe_2O_3$, $Al_2O_3$, $Cr_2O_3$, etc., and metals, such as: Fe, Ni, and Mn.

According to the temperature profile of the Earth's interior, the center of the Earth is made of high-temperature material, which is the hottest point, estimated to be 7000°C [Kubala & Mahan 1996], which is hotter than the surface of the Sun. The chemical components in the F-layer may reduce the viscosity; the full fluid oxides and metals can flow, diffuse, float, or sink more freely according to their specific gravity. Estimation of the Fe melting temperature at the ICB pressure based on static compression data spans the range 6230 ± 500°K [Anzellini, et al. 2013]. The F-layer above the ICB, in which Fe likes snowflakes falling in the inner core [Gubbins, Masters & Nimmo 2008].

A large amount of iron oxides (FeO, $Fe_2O_3$) is present in the mantle, and the deeper the mantle, the higher the proportion of iron oxides. An iron oxide with a metal-like density and electrical properties at high pressure and temperature exists in the Earth's core and may be a compromise between extreme views of the metallic phase and inconformity with the high cosmic abundance of oxygen [Altshuler & Sharipdzhanov 1971]. From this information, the outer core is rich in iron oxides.

In view of the topography, diffusion, inner core obstruction, tangential geostrophic flow, and toroidal flow affected the downward magma rich in iron oxides. Thus, the fluid flowed westward, which may have caused the secular geomagnetic variation. Under low viscosity, the oxides and metals can easily flow vertically and horizontally, allowing mutual oxidation-reduction reactions to occur in the F-layer. The active light metals take oxygen from the heavy metal oxides and are further oxidized into light metal oxides, whereas the heavy metal oxides are reduced to heavy metals and precipitate in the inner core. For example:

$Ca + FeO \longrightarrow CaO + Fe \downarrow$

$3Mg + Fe_2O_3 \longrightarrow 3MgO + 2Fe \downarrow$

$2Al + Fe_2O_3 \longrightarrow Al_2O_3 + 2Fe \downarrow$

$2Cr + 3FeO \longrightarrow Cr_2O_3 + 3Fe \downarrow$

$Mn + NiO \longrightarrow MnO + Ni \downarrow$

CaO, MgO, $Al_2O_3$, $Cr_2O_3$, and MnO float in the F-layer, and $Fe_2O_3$, FeO, and NiO become Fe and Ni, respectively, sinking down to form the inner core's main components. These oxidation-reduction reactions are exothermic processes that produce a large amount of heat. Reduced iron alloys with certain Ni concentrations settle at the ICB. The F-layer should be maintained through the interaction of the separated melting and solidifying regions distributed over the ICB [Alboussière, Deguen & Melzani 2010].

Kuroda (1956) declared that nuclear energy generated in the core from radioactive elements not only slows decay but also accelerates fission and demonstrated the feasibility of uranium ore seams engaging in a neutron induced nuclear fission chain. In 1972, French physicist Francis Perrin discovered the intact remains of a natural nuclear fission reactor in a uranium mine at Oklo, in the Republic of Gabon, that had operated just as Kuroda had predicted [Perrin 2018].

Herndon (1993) proposed a nuclear fission reactor at the center of the Earth, which may continue to the present through fuel breeding reactions. The magnitude of available nuclear fission energy release throughout geological time is of major geophysical importance and is sufficient to power the geomagnetic field. In August 2002, the Oak Ridge Lab of United States Federal Energy in National Geographic Society report a new achievement in scientific research that 6371 km below the surface of the Earth's center has a diameter of 8 km, consisting of uranium and plutonium fast-breed natural fission reactors, which can generate new fuel on their own and are a source of energy needed for all life on Earth.

The heat of oxidation-reduction reactions in the F-layer combines with the radiant heat generated by the decay

of radioactive elements in the outer core and with the nuclear fission heat that occurs from the Earth's center to surge up, becoming the main power source for the geo-dynamo of the consistent great convection cell of the Earth's internal material. In the F-layer, magma diffuses and absorbs a large amount of heat to rise to the CMB, where it condenses into solid rock as the process of a great convection cell starts anew (Figure 5).

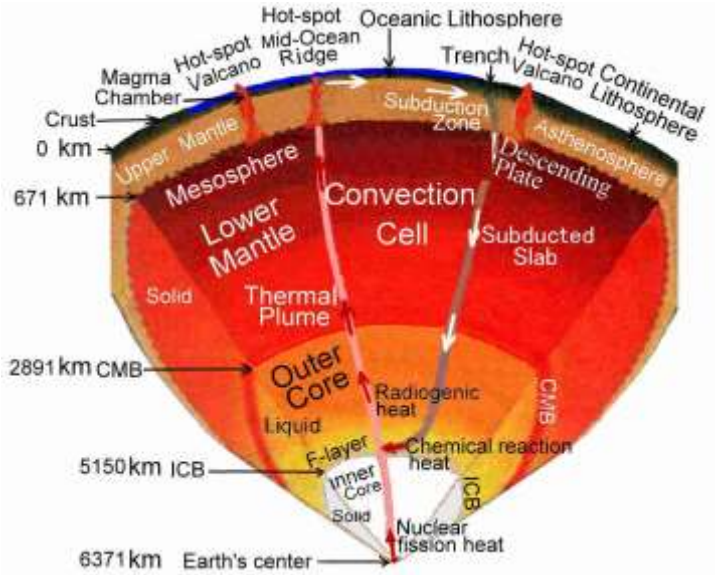


*Figure 5. Schematic diagram of the great convection cell, heat flow and composition of the Earth's interior.*

## IV. MATHEMATICAL FORMULATION

### 4.1 Digital evaluation of data in the new earth model

To calculate the Earth data, the density distribution follows the divisions of the PREM into 94 levels, including 82 thin shells. The thickness of each shell is not greater than 100 km and is so small compared with the Earth's radius of 6371 km that the density is linearly varied within it. Then, a simplified method is applied to calculate the Earth's information to simplify the calculation. The formula for the mass M of a uniform sphere can be derived as $M = (4/3)\pi\rho R^3$. The mass $\Delta M$ of each shell in the Earth's interior can be calculated as follows:

$$\Delta M = (4/3)\pi\rho_t R_t^3 - (4/3)\pi\rho_b R_b^3 \quad (1)$$

Where: $\rho_t$, $\rho_b$ are the densities at the top and bottom of a single shell, respectively, and $R_t$ and $R_b$ are the radii of the top and bottom of a shell, respectively. Because the difference between $R_t$ and $R_b$ is small and the density is regarded as a linear variation in the shell, the mean value $\overline{\rho}$ of both $\rho_t$ and $\rho_b$ is substituted for $\rho_t$ and $\rho_b$ in order to simplify the calculation. Then, Equation (1) becomes

$$\Delta M = (4/3)\pi\overline{\rho}(R_t^3 - R_b^3) \quad (2)$$

The moment of inertia $\Delta I$ of each shell in the Earth's interior can be calculated as follows:

$$\Delta I = (8/15)\pi\overline{\rho}(R_t^5 - R_b^5) \quad (3)$$

From fluid mechanics, the gradient of hydrostatic pressure in a region of uniform composition, which is in a state of hydrostatic stress, can be expressed as

$$dP/dR = -g\rho \quad (4)$$

Here, P and R are the pressure and radius, respectively, in the region; $\rho$ is the density at that depth; $g$ is the acceleration due to gravity at the same depth. If the effect of the Earth's rotation is negligible, the potential theory shows that $g$ is resulted only from the attraction of mass M within the sphere of radius R through

$$g = GM / R^2 \quad (5)$$

Where: G is the gravitational constant ($6.6726\times10^{-11} m^3/kg.s^2$). Equation (5) is substituted into equation (4) and integrated. To simplify the calculation, $\rho$ and M are substituted by $\overline{\rho}$ and $\overline{m}$, which are considered constants in

the thin shell and are irrelative to P and R. The result becomes

$\Delta P = (1/R_b - 1/R_t)G\overline{\rho}\,\overline{m}$ (6)

Where: ΔP is the difference in pressure between the top and bottom layers of the Earth, and $\overline{m}$ is the mass of a sphere as the mean value of the masses of the sphere within the top radius $R_t$ and the bottom radius $R_b$ a shell. Equation (6) cannot be applied to the Earth's center, where is a discontinuous point. The other form is applied to integrate the portion of the center as follows:

$\Delta Pc = (2/3)\pi G\overline{\rho}^2 R_c^2$ (7)

Where: ΔPc is the difference in pressure between the radius $R_c$ and the Earth's center at the central portion. The acceleration due to gravity g of each layer can be derived from equation (5). According to the observation data, the moment of inertia for the polar axis of the earth is $0.3309MeRe^2$ and about an equatorial axis is $0.3298MeRe^2$ [Garland 1979]. The earth is regarded as a sphere, of which the moment of inertia is determined to be $80286.4\times10^{40}$ g.cm$^2$ by taking the mean value of both figures, where Me is the earth's mass of $5974.2\times10^{24}$ g and Re is the equatorial radius of 6378.14 km.

To examine the accuracy of the applied equations, the density distribution of the PREM was used to calculate the Earth's mass, moment of inertia, pressure, and gravitational acceleration. The calculated values of the earth's data from the density distribution of the PREM compared with the values of the current data and the PREM are listed in Table 1 (http://newidea.org.tw/pdf/S60.pdf) and Table 2.

**Table 2**. Calculated values from the Earth's density distribution compared with the data, PREM, and current Earth.

| Data of the Earth | Mass | Moment of inertia | Pressure at CMB | Pressure at the Earth's center | Gravity at the CMB | Gravity at the Earth's surface |
|---|---|---|---|---|---|---|
| Unit | $10^{24}$ g | $10^{40}$g.cm$^2$ | K bar | K bar | cm/sec$^2$ | cm/sec$^2$ |
| PREM and current | 5974.200 | 80286.400 | 1357.509 | 3638.524 | 1068.230 | 981.560 |
| Calculated values | 5973.289 | 80205.664 | 1358.335 | 3655.973 | 1068.680 | 981.959 |
| Difference % | -0.0152 | -0.1006 | +0.0608 | +0.4796 | +0.0421 | +0.0406 |

The deviations of the calculated Earth's values from the PREM data and the current Earth are nearly within 0.1%, except for the pressure at the Earth's center, as shown in Table 2. This indicates that the calculated values are very close to the current data and that the simplified method is acceptable and useful; however, the calculated pressure of 3655.973 kbar at the Earth's center is 0.4796 % higher than the data of the PREM of 3638.524 kbar, which is about eight times the deviation at the CMB. We compared all the calculated pressures of the simplified method with those of the PREM using the deviation curve E in Table 3 (http://newidea.org.tw/pdf/S61.pdf), and Figure 6 shows the pressure P of the PREM.

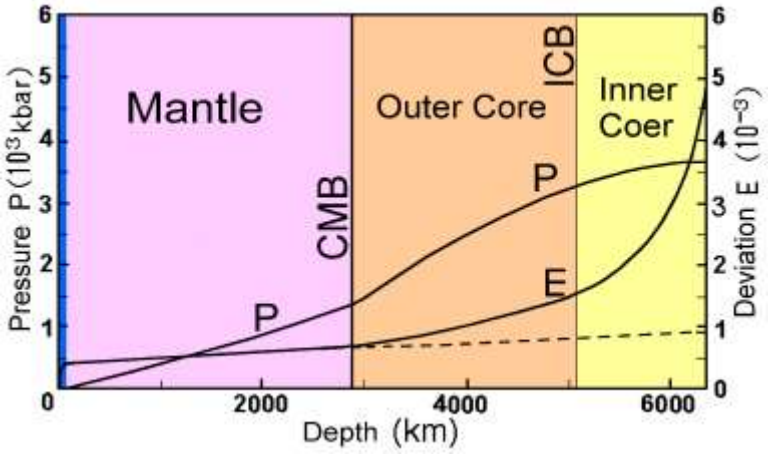


*Figure 6. The pressure P of the PREM and the deviation E of the calculated pressure using the simplified method*

*from the value of P.*

Figure 6 shows that the deviation E of the pressure curve from the crust to the CMB is nearly a straight line, indicating that the calculated pressures have systematic errors from the error theory. However, from the CMB to the Earth's center, the slope of curve E increases sharply above the dashed line, which is the straight line that extends from the CMB. This indicates a considerable discrepancy in the core. The structure of the PREM core, which greatly affects its core pressure, may be flawed.

To investigate the structure of the Earth, particularly the core, four density distribution curves are proposed to match the known conditions. The curves of density distribution from the crust to the CMB were adopted as the PREM, and four different plotted curves were assumed from the CMB to the ICB. Owing to a small jump in the P-wave velocity at the boundary of the F-layer in the outer core, the slope of the density curve was nearly as steep as that of the PREM. There is a discontinuity at the ICB, so a density jump of Derr's suggestion (2.0 g/cm$^3$) is used [Derr 1969]. In the inner core, the slope of the PREM density curve was the same. Figure 7 shows the four density curves of the assumed Earth model compared with the PREM.

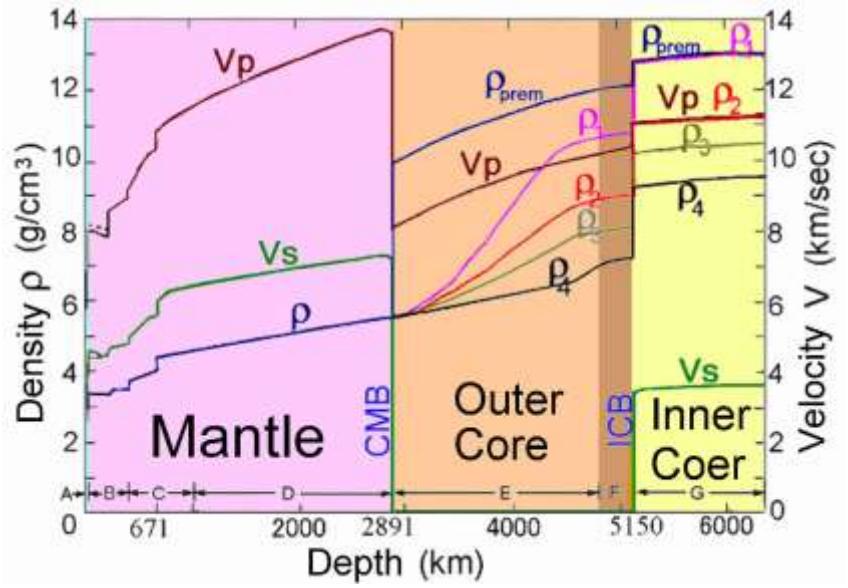


*Figure 7. These densities ρ of the new Earth models 1, 2, 3, and 4 were compared with those of the PREMs.*

The mass and moment of inertia of the four new Earth models can be determined and compared with the current measured data of the Earth's mass of $5974.2\times10^{24}$g and moment of inertia of $80286.4\times10^{40}$ g.cm$^2$, so the differences will be found to be very large, as shown in Table 4. The differences in the four new Earth models are the mass insufficiencies and the moment of inertia insufficiencies.

**Table 4**. The insufficiencies of Mass and moment of inertia in the four new earth models.

| Earth's Data | Unit | Observed value | New Model 1 | New Model 2 | New Model 3 | New Model 4 |
|---|---|---|---|---|---|---|
| Mass | $10^{24}$g | 5974.200 | 5409.024 | 5268.126 | 5204.761 | 5121.820 |
| Insufficiency | $10^{24}$g | - | 565.176 | 706.074 | 769.439 | 852.380 |
| Moment of inertia | $10^{40}$g.cm$^2$ | 80286.400 | 77007.472 | 76571.028 | 76378.768 | 76126.841 |
| Insufficiency | - | - | 3278.928 | 3715.372 | 3907.632 | 4159.559 |

Insufficiency in the Earth's mass and moment of inertia, called the missing mass and moment of inertia, are relative to the gravity of dark matter in astrophysics. It can only be obtained by comparing the Earth's observed data, which cannot be detected directly and answered clearly through ordinary Earth sciences. To solve the insufficiency problems, a new study of the Earth is attempted using contemporary physics. If we successfully explain that insufficient conditions exist under suitable conditions, a new Earth model will be established.

**4.2 Digital evaluation of data from the dark planet**

Proceeding with this assumption, the Earth's missing mass and moment of inertia are assumed to be those of cold dark matter (CDM), which may constitute a normal planet. To find a solution for this paper, dark matter is compared to Mars. The average radius of Mars is 3397 km, and the mass $642.40\times10^{24}$ g. Kaula and colleagues studied the moment of inertia of Mars and obtained the maximum allowable mean value is 0.3650 $MR^2$, i.e., $2689.8\times10^{40}$ g.cm$^2$ [Kaula, Sleep & Phillips 1989]. The insufficient data of 4 new Earth models roughly approach to the Mars'. So, the dark matter is considered a dark planet whose form is similar to that of Mars and whose characteristics are based on the inner planets of the solar system. To cut a figure of the dark planet, it is considered a sphere whose radius and density can be calculated using the simplified method from the insufficiencies in the Earth's mass and moment of inertia. The dark planet data can be calculated as follows:

Considering the density of rock on the Earth and Moon surfaces, a surface density of 2.70 g/cm$^3$of the dark planet is proposed. Under the condition that the density of a layer is proportional to its depth, a density trial value at the dark planet's center is selected. Applying Eqs. (2) and (3) to calculate the mass and moment of inertia of each shell, the total mass and moment of inertia of each shell can be obtained as follows:

The total mass and moment of inertia must correspond to the insufficiencies of the Earth's mass because the radius and center density of the dark planet are hypothetical values. Therefore, it is necessary to use a trial-and-error approach to determine the proper radius and center density.

Since the gravity of the dark planet may affect the Earth's orbit around the Sun, no abnormal effects on the Earth have been observed. It is assumed that the gravity centers of the Earth and the dark planet coincide at the same time. This is inferred from the phenomenon in which the same side of the Moon always faces the Earth, indicating that the Earth and the dark planet may rotate synchronously.

Assuming that the gravity centers of the Earth and the dark planet coincide at a single point and both rotate synchronously, the total mass and moment of inertia may be obtained from the following equation:

The mass of the Earth and the dark planet within its radius affects the gravity of each shell inside the Earth. The pressure difference $\Delta P'$ between the top and bottom of a shell on Earth is calculated as follows:

$$\Delta P' = ( 1/R_b - 1/R_t )G\overline{M}'\overline{\rho} \qquad (8)$$

Where: $\overline{M}'$ is the mean value of the total mass of the Earth and the dark planet within the radius $R_t$ and $R_b$.

Equation (8) cannot be applied to the center of the Earth. The average density $\overline{\rho}'$ of the central portion, combined with the Earth and the dark planet within radius $R_c$, can be calculated as follows:

$$\overline{\rho}' = ( M_C + M_d ) / [(4/3)\pi R_C^3] \qquad (9)$$

Where: Mc and Md are the masses of the central portion of the Earth and the dark planet, respectively.

The difference in pressure $\Delta P_c'$ between the top and center of the central portion of Earth can be obtained as follows:

$$\Delta P_c' = (2/3)\pi G\overline{\rho}\overline{\rho}'Rc^2 \qquad (10)$$

Based on the characteristics of the inner planets of the solar system, except for Mercury, a larger-radius planet has a higher average density. Therefore, the radius and average density of a suitable dark planet must be compatible with the inner planet's characteristics in the solar system. The data of the four new Earth models and each dark planet were compared with the data of the current Earth and the PREM (Table 5).

**Table 5:** Calculated data of the four new earth models compared with the data of the current earth and the PREM.

| Type of Earth's model | The Earth | | | | | | | The dark planet | | | | | Suitability |
|---|---|---|---|---|---|---|---|---|---|---|---|---|---|
| | Radius | Average density | Mass | Moment of inertia | Center density | Center pressure | Coefficient | Radius | Average density | Mass | Moment of inertia | Coefficient | |
| Unit | km | $g/cm^3$ | $10^{24}g$ | $10^{40}$ $g.cm^2$ | $g/cm^3$ | kbar | C | km | $g/cm^3$ | $10^{24}g$ | $10^{40}$ $g.cm^2$ | C | |
| PREM | 6371 | 5.5150 | 5974.200 | 80286.400 | 13.08848 | 3638.524 | 0.3309 | | | | | | |
| Model 1 | 6371 | 4.9945 | 5409.024 | 77007.472 | 13.08848 | 3283.754 | 0.3508 | 3808.414 | 2.4427 | 565.176 | 3278.928 | 0.4000 | no |
| Model 2 | 6371 | 4.8635 | 5268.126 | 76571.028 | 11.29785 | 3039.584 | 0.3581 | 3732.304 | 3.2421 | 706.074 | 3715.372 | 0.3777 | no |
| Model 3 | 6371 | 4.8050 | 5204.761 | 76378.768 | 10.46002 | 2934.587 | 0.3615 | 3717.755 | 3.5747 | 769.439 | 3907.632 | 0.3674 | no |
| Model 4 | 6371 | 4.7284 | 5121.820 | 76126.841 | 9.49821 | 2805.297 | 0.3662 | 3700.375 | 4.0161 | 852.380 | 4159.559 | 0.3564 | good |

The precise data for the Earth and the dark planet were calculated from the density distribution of the new Earth model 4. Tables 6 (http://newidea.org.tw/pdf/S62.pdf) lists the data for the Earth planet, Table 7 (http://newidea.org.tw/pdf/S63.pdf) lists the data for the dark planet, and Table 8 (http://newidea.org.tw/pdf/S64.pdf) lists the global data for the new Earth model. The pressure P and the acceleration due to gravity g of the new Earth model compared with the PREM are shown in Figure 8.

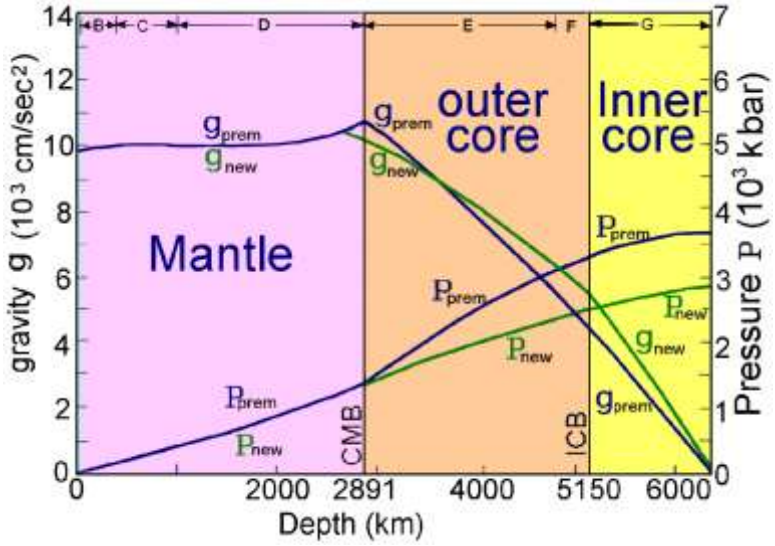


*Figure 8. Diagram of the gravity g and the pressure P of the new Earth model compares to PREM.*

Mars has an average radius of 3397 km, the mass 642.40×1024 g, and an average density of 3.912 $g/cm^3$. Both values of the radius and the average density of the dark planet in the new Earth model 4 are larger than those of Mars; therefore, this model is more suitable.

In this suitable model, the slope of the density curve from a depth of approximately 400 km of the upper mantle through zones C, D, and E to the upper boundary of the F-layer is nearly a straight line, which means that the density increases in proportion to its depth in accordance with general physical phenomena. Therefore, the new Earth model 4 is considered the proper new Earth model. The pressure curve of the new Earth model is smoother than that of the PREM below the CMB. In the gravity curve of the new Earth model, there are two deflection points in the curve: one is at 2670.625 km deep at the radius of the dark planet, and the other is at the ICB. The Earth has a mass of $5121.820\times10^{24}g$, a moment of inertia of $76126.841\times10^{40}$ $g.cm^2$, and an average density of 4.7284 $g/cm^3$. The Earth's center has a density of 9.49821 $g/cm^3$ and the pressure of 2805.297 kbar. The reduced values of the Earth's data relative to the current Earth are due to the existence of the dark planet. The dark planet has a radius of 3700.375 km, a moment of inertia of $4159.559\times10^{40}g.cm^2$, an

average density of 4.0161 g/cm$^3$and a mass of 852.380×10$^{24}$g about 1.33 times that of Mars. Table 8 lists the data for the new Earth model compared with those of the current Earth and the PREM

**Table 8.** The data of the new earth model are compared with those of the current earth and the PREM.

| Data of the planet | Radius | Mass | Inertia of moment | Average density | Center density | Center pressure | Coefficient |
|---|---|---|---|---|---|---|---|
| Unit | km | $10^{24}$g | $10^{40}$ g.cm$^2$ | g/cm$^3$ | g/cm$^3$ | kbar | C |
| PREM and current Earth | 6371.000 | 5974.200 | 80286.400 | 5.515 | 13.08848 | 3638.524 | 0.3309 |
| Earth planet | 6371.000 | 5121.820 | 76126.841 | 4.7284 | 9.49821 | 2805.297 | 0.3662 |
| Dark planet | 3700.375 | 852.380 | 4159.559 | 4.0161 | 7.96097 | 1115.272 | 0.3564 |

The density of the Earth's center was 9.49821 g/cm$^3$, which is much lower than the density of 13.08848 g/cm$^3$of the PREM. The pressure was 2805.297 kbar, which is much lower than the pressure of the PREM (3638.524 kbar). The composition of the inner core is predominantly Fe with a small amount of alloyed Ni. From the pressure-density Hugoniot data, the density of iron under 2805.297 kbar of pressure is approximately 12.7 g/cm$^3$ [Ahrens 1980], which is 25% greater than that of the new Earth model by 25%. The inner core is not pure iron but contains a significant fraction of light components [Ringwood 1984; Jephcoat & Olson 1987], which explains why the density of the inner core is much lower than the current value. Therefore, the composition of the inner core is predominantly Fe, alloyed with a small amount of Ni, and combined with a significant number of oxides.

## V. EXPLORING THE DARK ENERGY

### 5.1 Dark energy should be the universe's residual energy after the Big Bang

Lemaître (1927) proposed "The Big Bang Theory". At the beginning of the Big Bang, the universe was made up of high-temperature and hot energy with uniformity and isotropy. When this hot energy expands rapidly outward, an exponential inflation occurs [Guth 1982]. As the universe expands rapidly and temperature decreases, the distribution of energy changes slightly, according to Einstein's famous equation ($E = MC^2$) for gradual energy and mass interchange, creating the earliest substances. In 1964, the discovery of the cosmic microwave background by radio astronomers Penzias and Wilson was the most important evidence to test the Big Bang theory [Penzias & Wilson 1965]. Then, more and more astronomical and physical evidence came out, such as Cosmic Background Explorer (COBE) [Bennet 1993], WMAP, and Planck Satellite, when their detected spectrum was measured to map its black body radiation curve, the Big Bang Theory became more complete, and scientists believed in it.

In 2018, the Planck satellite detected tiny temperature fluctuations in the universe's radiation. These fluctuations reflect the baryon density of the universe before the formation of galaxies. Normal matter from galaxies and stars accounts for only 4.94 % of the universe's composition, with the rest missing substances, including dark matter, which accounts for 26.64 %, and mysterious dark energy, which accounts for 68.42% [Aghanim, et al. 2020]. Dark energy is one of the most mysterious phenomena in current physics. To investigate the dark energy, we applied the table of cosmological parameters of the WMAP results and Planck satellite results, whose Hubble constants nearly gradually decrease. We selected one set at each detection and are shown as follows.

**Table 9.** The cosmological parameter data were obtained from WMAP results and Planck satellite results.

| Source / Symbol | 1-year WMAP [Spergel et al. 2003] | 3-year WMAP [Spergel et al. 2007] | 5-year WMAP [Komatsu et al. 2009] | 7-year WMAP [Komatsu et al. 2011] | 9-year WMAP [Bennett et al. 2013] | Planck 2013 [Ade et al. 2014] | Planck 2015 [Ade et al. 2016] | Planck 2018 [Aghanim et al. 2020] |
|---|---|---|---|---|---|---|---|---|
| $H_0$ | 71.0 | 70.4 | 70.5 | 70.2 | 70.0 | 68.14 | 67.31 | 67.32 |
| $\Omega_b h^2$ | 0.0224 | 0.02186 | 0.02267 | 0.02255 | 0.02264 | 0.022242 | 0.02222 | 0.02238 |
| $\Omega_c h^2$ | – | – | 0.1131 | 0.1126 | 0.1138 | 0.11805 | 0.1197 | 0.12011 |
| $\Omega_m h^2$ | 0.135 | 0.1324 | 0.1358 | 0.1352 | 0.1364 | – | – | 0.14314 |
| $\Omega_\Lambda$ | 73.22% | 73.2% | 72.6% | 72.5% | 72.1% | 69.64% | 68.5% | 68.42% |
| $\Omega_m$ | 26.78% | 26.8% | 27.32% | 27.43% | 27.9% | 30.36% | 31.5% | 31.58% |
| $\Omega_b$ | 4.44% | 4.41% | 4.56% | 4.58% | 4.63% | 4.79% | 4.9% | 4.94% |
| $\Omega_c$ | 22.34% | 22.39% | 22.8% | 22.9% | 23.3% | 25.43% | 26.42% | 26.64% |
| $\Omega_v$ | 0.02% | 0.08% | 0.10% | 0.08% | 0.04% | 0.14% | – | – |
| $\Omega_{tot}$ | 1.020 | 1.08 | 1.099 | 1.080 | 1.037 | – | – | – |
| $t_0$ | 13.70 | 13.73 | 13.72 | 13.76 | 13.74 | 13.784 | 13.80 | 13.80 |

Taking the cosmological parameters of Planck 2018 results VI as the current situation of the universe, we have a description of parameter symbols and definitions and denote as follows:

$\Omega_b h^2$: Physical baryon density
$\Omega_c h^2$: Physical density of cold dark matter
$\Omega_m h^2$: Physical Matter density
$\Omega_\Lambda$: Dark energy density /critical density
$\Omega_m$: density of physical matter /critical density
$\Omega_b$: Physical baryon density /critical density
$\Omega_c$: Physical cold dark matter density /critical density
$\Omega_v$: massive neutrinos density /critical density
$\Omega_{tot}$: The total mass-energy density of the universe

$t_0$: Age of the universe (Gyr)
$H_0$: Hubble's constant (100 h km/Mpc·s)
1 megaparsec (Mpc) = $3.09\times10^{19}$ km
$h = H_0/100$
$\Omega_b = \Omega_b h^2 / (H_0/100)^2$
$\Omega_c = \Omega_c h^2 / (H_0/100)^2$
$\Omega_m = \Omega_m h^2 / (H_0/100)^2$
$\Omega_{tot} = \Omega_\Lambda + \Omega_m$
$\Omega_m = \Omega_b + \Omega_c + \Omega_v$, (some $\Omega_v$ include in $\Omega_b$)

According to the table of cosmological parameters from WMAP results and Planck Satellite results, the dark energy density ΩΛ from 1-year WMAP results (Spergel, et al. 2003) to Planck 2018 results VI (Aghanim, et al. 2020) for 15 years, the value from 73.22% decreases gradually down to 68.42%, decreasing 4.8%, but the value of total matter density $\Omega m$, increases gradually from 26.78% up to 31.58%, increasing 4.8%. As the universe expands rapidly, the temperature drops and gradually cools down. Then, energy transforms into the building blocks of matter. From the table, the loss of dark energy is equal to the increase in total matter, which is consistent with the narration of the Big Bang Theory.

Taking the cosmological parameters of Planck's 2018 results VI as the current situation of the universe, we may imagine that at the first time of the Big Bang, the full energy (100% energy density) of the universe gradually loses. After 13.8 billion years, the energy density remains at 68.42%, which is called dark energy density, and 31.58% of the total matter density is created. According to the Big Bang Theory, we should take the current dark energy as the residual energy of the universe after the Big Bang.

**5.2 Accelerating the expansion of the universe can be interpreted through 3-cosmic framework**

After WMAP and Planck satellite detection, the current actual temperature of cosmic microwave background radiation (CMBR) in our cosmos is only 2.725 °K, which is awfully close to absolute zero (0°K = −273.15°C); therefore, the energy of our cosmos is so poor that it cannot contribute to an accelerating expansion of the universe.

According to Table 9, cold dark matter density from 1-year WMAP results to Planck 2018 results VI, the value from 22.34% increases gradually up to 26.64%, increasing 4.3%, and baryon (normal matter) density in our cosmos from the value 4.44% increases gradually up to 4.94%, only increasing 0.5%, which compares to increasing rate of cold dark matter density, the ratio is about 1/8.6. The temperature is a display of the thermal motion of microscopic particles; therefore, the hot temperature must display its high energy. The increasing baryon density value is so small that the energy in our cosmos is so poor that we can call ours a low-energy-density cosmos; on the contrary, the increasing cold dark matter density are so large that we can call it high-energy-density cosmoses, which are the cosmoses other than ours.

Under the situation of 3-cosmic framework of the universe after the Big Bang, the dark energy density of 68.42% is the remainder today, but the lost 31.58% transforms into total matter density, which contains a baryon density of 4.94% in our cosmos and the cold dark matter density of 26.64% in other cosmoses. Because the current dark energy density of 68.42% is bigger than the total matter density of 31.58%, which is about 36.84%; therefore, a large amount of dark energy will certainly cause the universe to expand rapidly, which means that the universe is still in a high-energy state and can expand rapidly. Under the 3-cosmic framework of the universe, the rate of expansion in a high-energy-density cosmos will be much higher than that in a low energy density cosmos, such as ours.

Based on the String Theory, the fundamental interaction forces of nature, except the gravitational force, cannot penetrate into the other cosmos; therefore, the energy of one cosmos cannot affect the other cosmos. As a result, the dark energy of high-energy-density cosmoses cannot directly contribute to the expansion of our low-energy-density cosmos. However, when the high-energy-density cosmoses expand more rapidly than our low-energy-density cosmos, its matter (i.e., dark matter for our cosmos) will expand at the same pace, which meanwhile uses its gravity to drag the stars and galaxies of our low-energy-density cosmos away at the same pace to expand. In our view, this is the effect of tugging stars and galaxies of the universe at accelerating expansion.

## VI. DISCUSSION

### 6.1 Quantum experiments indicate the existence of a multiverse in space

In classical physics, matter is made up of particles, which are entities that conform to a simple orbit and can calculate their motion, velocity, angle, and speed at any one time; for example, an elementary particle in atom – electron, in Newton's classical mechanics, rotates around the nucleus in a circular orbit, and the position, momentum, and orbit of each particle is fully predictable, and it is only in a single place at the same time. This idea is similar to the case in our solar system, but beginning in the 1920s, quantum experiments have shown that in the atomic structure, quantum physicists tried to describe the “electrons” of the elementary particles accurately. They found that it was almost impossible because it did not have a fixed position and the particles could indeed appear in different places at the same time, just as it has fractals, but when they actually look at it, they can only find it in one location. However, in quantum mechanics, the position and momentum of each elementary particle is expressed by a static, spherical wave function around the nucleus, which can only be counted by probability or statistics. In other words, the elementary particles do not remain in a stable orbit but appear intermittently in many places. The only explanation is that the particles not only exist in our cosmos but also sweep through other cosmoses, indicating the existence of multiple cosmoses in space, i.e., the multiverse exists.

In the multiverse, there are no basic interactive forces of nature except gravity, i.e., the graviton in the field of gravity can penetrate all the cosmoses, i.e., gravity affects each other’s orbits of stars, but electromagnetic forces (light) do nothing to each other, i.e., the stars among the multiple cosmoses are invisible to each other. Because many compact objects of the other binary cosmoses cannot be seen, the phenomenon of gravity attraction among the triple cosmoses is the phenomenon of dark matter. Therefore, dark matter should be situated in cosmoses other than ours; in other words, the multiverse should hold dark matter.

### 6.2 The Chandler wobble confirms a dark planet inside the Earth but in another cosmos

Directly examining the existence of dark matter is difficult; however, that can be recognized from Chandler wobble.

Referring to the orientation of the Earth's rotation axis in space in addition to both precession and nutation, a wobble occurs on the Earth's instantaneous axis of rotation. The wobble alters the position of a point on the Earth relative to the pole of rotation. Chandler (1891) pointed out two distinct kinds of wobble periods. The first is a period of 12 months, and the second is a period of 433 days, which is approximately 14 months. The former, called annual wobble, is affected by the seasonal climate. The latter, called the Chandler wobble, has not been solved for more than one hundred years. The Chandler wobble is a small deviation that changes by approximately nine meters at the point on the surface of the Earth's rotation axis.

Gross (2000) found that two-thirds of the Chandler wobble was caused by fluctuating pressure on the seabed, which, in turn, is caused by variations in temperature, salinity, and wind that alter the ocean circulation. The remaining third is due to atmospheric fluctuations. The full explanation of this period also involves the fluid nature of the Earth's core and oceans. The wobble produces a negligible ocean tide with an amplitude of approximately 6 mm, called a "pole tide", which is the only tide not caused by an extraterrestrial body. While it has to be maintained by changes in the mass distribution or angular momentum of the Earth's outer core, atmosphere, oceans, or crust (from earthquakes), the actual source was unclear for a long time because no available motions seemed to be coherent with what was driving the wobble.

This is inferred from the phenomenon in which the same side of the Moon always faces the Earth, indicating that the Moon and Earth rotate synchronously. The same phenomenon will happen to the Earth and the dark planet in which both rotate synchronously, but the rotation axes of both are impossible to coincide with each other, i.e., an angle between the two rotation axes produces the Chandler wobble as the precession and nutation due to the effects of the Sun and Moon on non-parallel rotation axes with the Earth's. Therefore, the effect of Chandler wobble should confirm the existence of a dark planet inside Earth but in a cosmos other than ours.

**6.3 The existence of dark matter can solve the problems of astronomical observations in the universe**

From this study, the hypothesis of the three-cosmic framework of the universe should enable a new way to discover abundant dark matter and solve some astrophysical problems. There were two early observations of astrophysicists, as follows:

1. Cygnus X-1 is a hot super giant star orbited by an invisible compact object in 5.6 days [Stokes & Michalsky 1979]. The mass of the compact object can be estimated from the Doppler shifts in the visible super giant stars' spectrum. Its mass is about 9 times of the sun. This is considerably greater than the maximum mass of a neutron star. Therefore, the compact object is neither a neutron star nor a white dwarf star. Since it has problems of optical confirmation, the compact object may not be a black hole. If we consider the compact object of Cygnus X-1 as the dark matter in a cosmos other than ours and its gravity affects Cygnus X-1, the problem may be solved.
2. Stars that evaporate from the Hyades cluster will remain within a few hundred parsecs (pc) (1 parsec = 3.26 light year) of the cluster if they are dynamically bound to a much more massive entity containing the cluster. A local mass enhancement of at least (5-10)×$10^5$ solar masses, with a radius of approximately 100 pc, can trap stars with an origin related to that of the Hyades cluster and explains the excess of stars with velocities near the Hyades velocity that constitutes the Hyades supercluster. A portion of this mass enhancement can occur in visible stars, but a substantial fraction is probably in the form of dark matter [Casertano, Iben & Shilds 1993]. This dark matter should be in a cosmos other than ours.

**6.4 The existence of a dark planet X can solve the problems of astronomical observations in the solar system**

In the 1970s, Joseph Brady published records of the observation of Halley's Comet and found that its approach to the Sun has always been erroneous at 3 or 4 days in the predicted time of the perihelion passage. The prediction of Halley's Comet, Brady, was based on studies of periods of Halley's Comet using old European and Chinese records. A computer was used to treat the data in a numerical model of the solar system. He has been able to predict an invisible X planet (trans-plutonian planet) that affects the orbit of Halley's Comet. It was about three times the size of Saturn, with a highly inclined orbit (i = 120°, e = ± 0.07) to the ecliptic and a period of 450 years [Brady 1971, 1972].

In the 1980s, scientists discovered that Uranus and Neptune were pulled off and deviated from the normal orbit by an unknown force in the solar system. This unknown force may have come from an unknown planet, with its

gravity disturbing these two giant planets. Flandern (1981) proposed a search for an X planet, which has about three times the mass of the Earth and a highly inclined eccentric orbit that accounted for all the perturbations on the motions of Neptune.

NASA research scientist Anderson (1988) presented the deviation of Neptune and Uranus in the regular orbit from observed astronomical data of the 19th century and proposed "The Theory of X Planet". The mass of planet X is about five times that of Earth, and its period is about 700～1000 years. The orbit is elliptical, and the inclination from the orbit to the ecliptic is large and almost perpendicular. The planet X has been searched for, but it remains to be found.

Pioneer 10 and 11 spacecraft were launched in 1973 and 1974 respectively. When the spacecrafts approached Neptune and Uranus, unknown objects were found that could affect their operations. In 2002, John Anderson and colleagues' previous analyses of radio Doppler and ranging data from distant spacecraft in the solar system indicated that an apparent anomalous acceleration is acting on Pioneer 10 and 11, with a magnitude about $8\times10^{-8}$ cm/s$^2$, directed toward the Sun. The effect is clearly significant and remains to be explained. Pioneer 10 has assessed all known mechanisms and theories, but has so far found nothing and cannot explain the mystical power of this universe; the probe has revealed an unknown force. The existing cosmology and space navigation theory will face a significant impact [Anderson, et al. 2002].

In 2006, Pluto was reclassified as a dwarf planet, removing it from the list of major planets in our solar system. In 2016, astronomers proposed a Planet Nine based on the peculiar clustering of the orbits of several extreme trans-Neptunian objects (ETNOs), which proposes that a larger object is shepherding them. This gravitational influence proposes an unseen, massive planet in the distant outer solar system. The search for Planet Nine continues. As of 2024, the semi-major axis of Planet Nine is estimated to be 290 ± 30 AU, implying that the planet has an orbital period of 4,190~5,720 years and has 4.4 ± 1.1 times the mass of Earth [Siraj, Chyba & Tremaine 2025]. Astronomers use new observatories, such as Vera C. Rubin Observatory to search Planet Nine, but there is no direct evidence yet.

If we consider a dark planet X or a dark planet Nine, which orbits around the Sun in a cosmos other than ours, then its gravity will sometimes affect the motion of the Halley's Comet, Neptune, Uranus, Pioneer 10 and 11 spacecrafts and the gravitational influence of ETNOs. Therefore, the invisible object problem may be solved, which can solve the problems of astronomical observation in our solar system.

**6.5 Dark matter and dark energy interaction dominates the fate of the universe**

Scientists assume that dark energy is the force that tears apart the universe, but the gravity of dark matter condenses everything, and the two forces act mutually on that dark matter and dark energy dominate the fate of the universe and form the structure of the universe as we know it today. Energy causes the universe to expand because of its hot temperature, but matter causes each other to shrink because of gravity. However, from the data of 2018 Planck results VI, the current dark energy density of 68.42% is bigger than the total matter density of 31.58%, which is about 36.84%; therefore, this much dark energy will certainly put the universe in rapid expansion.

As a result of the discovery of the 1a supernova, scientists speculate that the universe continues to expand, and the speed is expanding faster and faster, and the structure of space-time is unable to maintain the integrity of the universe, making it colder and colder. Expansion keeps neighboring stars away and becomes increasingly lonely, and becomes isolated star-and-planet, until the star's nuclear reactor runs out of fuel, tearing up the entire star system to the point where it tears up matter itself, breaking the chemical bond, every atom of everything is torn apart, everything is broken down into elementary particles, leaving a dead-end remnant, and that is the end of the universe — the "Big Rip" [Ellis, et al. 2012].

Our universe will eventually form an icy world of eternal complete silence, with no living thing to exist, and scientists estimate that it will take at least fifty billion years to happen. The universe is expanding faster and faster, keeping galaxies farther apart, and is expected to tear the universe apart, as if it were going to win the cosmic war. The accelerating expansion of the universe is different from "Dao", which came from the well-known Chinese philosopher Lao-tzu's "Dao De Ching" in the Spring and Autumn Period (about 2500 years ago). In chapter 25 of "Dao De Jing", it is described as follows: "Something is blended, which is born peacefully and scarcely before the

universe appears, independent without change, revolving around without losing it and can be the mother of the world". I don't know its name, it is called **'**Dao**'**……, Man obeys the Earth, the Earth obeys Heaven, Heaven obeys Dao, and Dao obeys Nature**"**. The regular way "Dao" of the universe must also be revolved around without losing it; in other words, the regular way of the universe must be revolved around to fit in and should not form an icy world that is forever dead, so scientists' presumption needs to be studied further.

On the other hand, according to the Big Bang Theory, dark energy will gradually decrease, but total matter will gradually increase. When the dark energy density decreases to below 50% or less, and the total matter density increases to greater than 50% or more, the universe may stop expanding and turn around to collapse in a **"**Big Crunch**"** due to gravity.

## VII. CONCLUSION

After studying the existence of a dark planet, which is located in the interior of the Earth but in another cosmos than ours, it should serve as a proof of the existence of dark matter and confirm the multiverse. Based on the applications of ten-dimensional space-time of original String Theory and combining with Anthropic Principle and Causality, a 3-cosmic framework in the universe is developed, i.e., triple cosmoses, which can identify dark matter and dark energy, including the accelerating expansion of the universe. This framework should enable a new approach to breaking the bottleneck of research in the space of the universe, but it still needs to be proved by the fine outcomes of physicists' new research.

## VIII. REFERENCES


1. Ade, P. A. R., et al. (Planck Collaboration). (2014). Planck 2013 results. Overview of the products and scientific results, *Astronomy and Astrophysics,* 571(A1), Table 10. Cosmological parameter values for the Planck-only best-fit 6-parameter ΛCDM model and for the Planck best-fit cosmology including external data sets, Planck (CMB + lensing), Best fit.
2. Ade, P. A. R., et al. (Planck Collaboration). (2016). Planck 2015 results. XIII. Cosmological parameters, *Astronomy and Astrophysics,* 594(A13): 32, Table 4. The parameters of the base ΛCDM cosmology computed from the 2015 baseline Planck likelihoods, Planck TT+ low P.
3. Aghanim, N., et al. (Planck Collaboration). *(*2020). Planck 2018 results. VI. Cosmological parameters, *Astronomy & Astrophysics*, 641(A6): 7, Table 1). Base-ΛCDM cosmological parameters from Planck TT, TE, EE + lowE + lensing, and Plik best fit.
4. Agnew, D., Berger, J., Buland, R., Farrell, W. & Gilbert, F. (1976). International Deployment of Accelerometers: a network for very long period seismology, *EOS, Trαns. Am. Geophys. Union*, 57: 180-188.
5. Ahrens, T. J. (1980). Dynamic Compression of Earth Materials, *Science*, 207: 1035.
6. Alboussière, T., Deguen, R. & Melzani, M. (2010). Melting-induced stratification above the Earth's inner core due to convective translation, *Nature*, 466: 744-747.
7. Altshuler, L. V. & Sharipdzhanov, L. V. (1971). On the distribution of iron in the Earth and the chemical distribution of the latter. *Bull. Acad. Sci. USSR Geophys. Ser*. 4: 3-16.
8. Anderson, J. D., et al. (2002). Study of the anomalous acceleration of Pioneer 10 and 11. *Physical Review D*, April 11, 2002, 65: 082004, LA-UR-00-5654.
9. Anderson, John. (1988). Planet X: Fact or Fiction? *Planetary Reports*, 8 (4): 6-9.
10. Anzellini, S., Dewaele, A., Mezouar, M., Loubeyre, P. & Morard, G. (2013). Melting of Iron at Earth's Inner Core Boundary Based on Fast X-ray Diffraction, *Science*, 340 (6131): 464-466.
11. Aubert, J., Amit, H., Hulot, G. & Olson, P. (2008). Thermochemical flows couple the Earth's inner core growth to mantle heterogeneity, *Nature*, 454: 758-762.
12. Bartusiak, M. (1988). Wanted: Dark Matter, *Discovery*, Dec. 1988, 63-69.
13. Bennett, C. L., et al. (1993). Scientific results from the Cosmic Background Explorer, *PNAS.* 1993; 90(11):4766-4773.
14. Bennett, C. L., et al. (2013). Nine-Year Wilkinson Microwave Anisotropy Probe (WMAP) Observations:

Final Maps and Results, *The Astrophysical Journal Supplement Series,* 208(2): 46, p. 17 WMAP: Cosmological Parameter Summary.

15. Bergman, M. I. (2003). Solidification of the Earth's core, in Earth's Core: Dynamics, Structure, Rotation, *Geodyn. Ser.*, 105-127.
16. Bloxham, J. & Jackson, A. (1990). Lateral temperature variations at the core-mantle boundary deduced from the magnetic field, *Phys Rev Lett,* 17: 1997-2000.
17. Bloxham, J., Gubbins, D. (1987). Thermal core-mantle interactions, *Nature*, 325: 511-513.
18. Bolt, B. A. (1972). The density distribution near the base of the mantle and near the Earth's center, *Phys. Earth Planet. Inter.*, 5: 301-311.
19. Bolt, B. A., Qamar, A. (1970). Upper bound to the density jump at the boundary of the Earth's inner core, *Nature*, 228: 148-150.
20. Boschi, L. and Dziewonski, A. M. (1999). High- and low- resolution images of the Earth's mantle: Implications of different approaches to tomographic modeling, *Journal of Geophysical Research*, 104 (B11): 25567- 25594.
21. Boschi, L., Dziewonski, A. M. (2000). Whole Earth tomography from delay times of P, PcP, and PKP phases lateral heterogeneities in the outer core or radial anisotropy in the mantle? *J. Geophys. Res.*, 105: 13675-13696.
22. Brady, J. L. (1971). The orbit of Halley's Comet and apparition of 1896, *Astronomical Journal,* 76 (8): 728-739.
23. Brady, J. L. (1972). The Effect of Trans-plutonian Planet on Halley's Comet, *Publication of the Astronomical Society of the Pacific,* 34 (498): 314-322.
24. Buchbinder, G. G. R. (1968). Properties of the Core-Mantle Boundary and Observations of PcP, *J. Geophys. Res*., 73: 5901–5912, 2012.
25. Bullen, K. E. & Bolt, B. A. (1986). An Introduction to the Theory of Seismology, 4th Ed., *Geophysical Journal of the Royal Astronomy Soc*., 86 (1): 215-216.
26. Byrne, P. (2008). The Many Worlds of Hugh Everett**,** *Scientific American*, on October 21, 2008.
27. Casertano, S., Iben, I. & Shilds, A. (1993). The Hyades Cluster-Supercluster Connection: Evidence for a Local Concentration of Dark Matter, *Astrophysical Journal*, Part 1, 410: 90-98.
28. Chandler, S. C. (1891). On the variation of latitude. *Astronomical Journal*, 11: 59-61, 65-70.
29. Choy, G. L. & Cormier, V. F. (1983). The structure of the inner core inferred from short-period and broad-band GDSN data, *Geophys. J. R. Astr. Soc.*, 72: 1-21.
30. Clowe, D., Bradac, M. & Gonzalez A. H., et al. (2006). A direct empirical proof of the existence of dark matter, *Astrophys J Lett*., 648(2): L109-L113.
31. Condie, Kent C. (1997). Plate tectonics and crustal evolution (4th ed.). *Butterworth-Heinemann*, 2005.
32. Cormier, V. F. (1981). Short-period PKP phases and the inelastic mechanism of the inner core, *Phys. Earth Plant Inter.* 24: 291-301.
33. Cormier, V. F. (2009). A glassy lowermost outer core. *Geophys. J. Int.*, 179: 374-380.
34. Cormier, V. F., Attanayake, J. & He, K. (2011). Inner core freezing and melting constraints from seismic body waves, *Earth Planet. Inter*., 188: 163-172.
35. Creager, K. C. & Jorden, T. H. (1986). A spherical structure of the core-mantle boundary from PKP travel time, *Geophys. Res. Lett*., 13: 1497-1500.
36. Derr, J. S. (1969). Internal Structure of the Earth Inferred from Free Oscillations, *J. Geophys. Res.*, 74: 5202-5220.
37. Deutsch, D. (2010). Apart from Universes / In Many Worlds? Everett: Quantum Theory and Reality. Saunders, S., Barrett, J., Kent, A., & Wallace, D. (eds.). *New York: Oxford University Press,* 542-552.
38. Doornbos, D. J. & Hilton, T. (1989). Models of the core-mantle boundary and the travel times of internally reflected core phases, *J. Geophys. Res.*, 94 (B11): 15,741-15,751.
39. Dvali, G. (2004). Out of the Darkness. *Scientific American*, February 2004, 68-75.

40. Dziewonski, A.M. & Anderson, D. L. (1981). Preliminary Reference Earth Model (PREM), *Phsy. Earth Planet, Inter.*, 25, 297-356.
41. Ellis, G. F. R., Martens, R., & MacCallum, M. A. H. (2012). Relativistic Cosmology. *Cambridge, UK: Cambridge University Press*. 146–147.
42. Everett, Hugh. (1957). Relative State Formulation of Quantum Mechanics, *Reviews of Modern Physics.* 29: 454-462.
43. Fiquet, G., Auzende, A. L., Siebert, J., Corgne, A., Bureau, H., Ozawa, H., Garbarino, G. (2010). Melting of peridotite to 140 gigapascals, *Science*, 329: 1516-1518.
44. Flandern, T. V. (1981). The renewal of the Trans-Neptunian planet search, *Bulletin of the American Astronomical Society*, 12: 830.
45. Forte, A. M. & Peltier, R. W. (1991). Mantle convection and core-mantle boundary topography: Explanations and implications, *Tectonophysics*, 187 (1-3): 91-116. https://doi.org/10.1016/j.tectonop.2018.01.013.
46. Garcia, R. & Souriau, A. (2000). Amplitude of the core-mantle boundary topography estimated by stochastic analysis of core phases, *Phys. Earth Planet. Inter.*, 117: 345-359.
47. Garland, G. D. (1979). Introduction to Geophysics, 2nd Ed., *W. B. Saunders Company*, Toronto, Canada. 4-8, 28-30, 44-46, 130, 387-389.
48. Gouranton, C. G., et al. (2025). GRACE Detection of Transient Mass Redistributions During a Mineral Phase Transition in the Deep Mantle, *Geophysical Research Letters*, 28 August 2025, Volume 52, Issue17. https://doi.org/10.1029/2025GL116408
49. Gross, Richard S. (2000). The Excitation of the Chandler Wobble, *Geophys. Res. Lett.*, 27 (15): 2329-2332.
50. Gubbins, D. & Richards, M. A. (1986). Coupling of the core dynamo and mantle: thermal or topography? *Phys Rev Lett*, 13: 1521-1524.
51. Gubbins, D., Masters, T.G. & Nimmo, F. (2008). A thermochemical boundary layer at the base of Earth's outer core and independent estimate of core heat flux, *Geophys. J. Int.*, 174: 1007-1018.
52. Guth, A. H. (1982). Fluctuation in the New Inflationary, *Physical Review Letters*, 49(15): 1110- 1113.
53. Hall, T. H. & Murthy, V. R. (1972). Comments on the Chemical Structure of a Fe-Ni-S Core of the Earth, *EOS.* 53 (5): 602.
54. Hand, E. (2015). Mantle plumes seen rising from Earth's core, *Science*, 349 (6252): 1032-1033.
55. Hecht, J. (1995). Buried treasure from the hot heart of the Earth, *New Scientist*, 19 (16).
56. Herndon, J. M. (1993). Feasibility of a nuclear fission reactor at the center of the Earth as the energy source for the geomagnetic field, *Journal of Geomagnetism and Geoelectricity*, 45 (5): 423–437.
57. Ho, Hsien-Jung. (2019). Based on the Space-Time of String Theory Exploring Dark Matter inside the Earth, *Journal of Scientific and Engineering Research*, 2019, 6(8): 166-191. http://newidea.org.tw/pdf/S71.pdf.
58. Ho, Hsien-Jung. (2022). The 3-Cosmic Framework of the Universe Can Hold Dark Matter and Dark Energy, *Journal of Scientific and Engineering Research*, 9(4), 67–77. https://doi.org/10.5281/zenodo.10518988.
59. Horton, F., et al. (2023). Highest terrestrial 3He/4He credibly from the core, *Nature,* 623:90–94.
60. Jeanloz, R. & Ahrens, T. J. (1980). Equations of FeO and CaO, *Geophysics. J. R. Astr. Soc.*, 62: 505- 528.
61. Jeanloz, R. & Wenk, H. R. (1988). Convection and anisotropy of the inner core, *Geophys. Res. Lett*. 2015; 15:72-75.
62. Jeanloz, R. (1990). The Nature of the Earth's Core, *Annu. Rev. Earth Planet. Sci.,* 18: 357-386.
63. Jeffreys, H. (1939). The times of the core waves, (Mon) *R. Astron. Soc. Geophys. Suppl*., 4: 498.
64. Jephcoat, A. & Olson, P. (1987). Is the Inner Core of the Earth Pure Iron? Nature, 325: 332-335.
65. Kapteyn, Jacobus Cornelius. (1922). First attempt at a theory of the arrangement and motion of the sidereal system, *Astrophysical Journal,* 55: 302-327.
66. Kaula, W. M.; Sleep, N. H. & Phillips, R. J. (1989). More about the Moment of Inertia of Mars, *Geophys Res Lett*, 16 (11): 1333-1336.

67. Kennett, B. L. N., Engdahl, E. R., Buland, R. (1995). Constraints on seismic velocities in the Earth from travel times, *Geophys. J. Int.*, 122: 108- 124.
68. Kerr, R. A. (1997). Deep-Sinking Slabs Stir the Mantle, *Science,* Retrieved 2013-06-13.
69. Knittle, E. & Jeanloz, R. (1991). The high-pressure phase diagram of $Fe_{0.94}O$: A possible constituent of the Earth's core, *J. Geophys. Res.*, 96: 16169-16180.
70. Knopoff, F. (1965). A preeminent seismology, *Phys. Rev*., 138 (A): 1445.
71. Komatsu, E., et al. (2009). Five-Year Wilkinson Microwave Anisotropy Probe (WMAP) Observations: Cosmological Interpretation, *The Astrophysical Journal Supplement Series*, 180(2): 371, p. 14 Comparison of ΛCDM Parameters from WMAP + BAO + SN with Various SN Compilations, Union.
72. Komatsu, E., et al. (2011). Seven-Year Wilkinson Microwave Anisotropy Probe (WMAP) Observations: Cosmological Interpretation, *Astrophys. J. Suppl. Ser.*, 192(2): 3, Table 1. Summary of the Cosmological Parameters of ΛCDM Model, WMAP+BAO+$H_0$ Mean.
73. Kubala, B. & Rao, M. (1996). Earth's Core Temperature, *Byrdand Black*.
74. Kuroda, P. K. (1956) On the Nuclear Physical Stability of the Uranium Minerals, *Journal of Chemical Physics* 25 (4): 781–782, p. 1295–1296.
75. Lay, T. (1989). Structure of the Core-Mantle Transition Zone: A Chemical and Thermal Boundary Layer, *EOS*, Jan., 70(4): 24, 49, 54-55, 58-59.
76. Leake, J. (2013). Cosmic map reveals the first evidence of other universes. *The Sunday Times,* May 19, 2013.
77. Lemaître, Georges. (1927). Un Univers homogène de masse constante et de rayon croissant rendant compte de la vitesse radiale des nébuleuses extra-galactiques, *Annales de la Société Scientifique de Bruxelles,* A47: 49-59.
78. Lyttleton, R. A. (1973). The end of the iron-core age, *Moon,* 7: 422-439.
79. McFadden, P. L., Merrill, R. T. (1995). History of Earth's magnetic field and possible connections to core-mantle boundary processes, *J. Geophys. Res.*, 100: 307-316.
80. McQueen, R. G., Marsh, S. P., Taylor, J. W., Fritz, J. N. & Carter, W. J. (1970). The equation of state of solids from shock wave studies, in high velocity impact phenomena, *Kinslow, R.*, *Academic Press, New York*, 294-419.*EOS*. 53 (5): 602.
81. Mersini-Houghton, L. (2008). Birth of the universe from the Multiverse, *Department of Physics and Astronomy*, *North Carolina University*, September 22, 2008.
82. Messling, N., Willbold, M., Kallas, L., Elliott, T., Fitton, J. G., Müller, T. and Geist, D. (2025). Ru and W isotope systematics in ocean island basalts reveals core leakage, *Nature,* 642, 376–380. https://doi.org/10.1038/s41586-025-09003-0.
83. Mjelde, R., Faleide, J. I. (2009). Variation of Icelandic and Hawaiian magmatism: evidence for co-pulsation of mantle plumes? *Mar. Geophys. Res.*, 30: 61-72.
84. Mjelde, R., Wessel, P., Müller, D. (2010). Global pulsations of intraplate magmatism through the Cenozoic, *Lithosphere*, 2 (5): 361-376.
85. Morelli, A., Dziewonski, M. (1987). Topography of the core-mantle boundary and lateral homogeneity of the liquid core, *Nature*, 19, Feb., 325: 678-683.
86. Morgan, W. J. (1971). Convection plumes in the lower mantle: *Nature,* 230: 42-43.
87. Morgan, W. J. (1972). Deep mantle convection plumes and plate motions, *Bull. Am. Assoc. Pet. Geol.*, 56: 203-213 (2019).
88. Mundl, A., et al. (2017). Tungsten-182 heterogeneity in modern ocean island basalts. *Science*, 356, 66–69. https://doi.org/10.1016/j.science.2017.01.013.
89. Mundl-Petermeier, A., et al. (2020). Anomalous 182 W in high 3He/4He ocean island basalts: fingerprints of the Earth's core? *Geochim. Cosmochim. Acta*, 271, 194–211.
90. Neuberg, J. & Wahr, J. (1991). Detailed investigation of a spot on the core mantle boundary using digital PcP data, *Phys. Earth planet. Inter.*, 68: 132-143.

91. Obayashi, M., Fukao, Y. (1997). P and PcP travel time tomography for the core-mantle boundary, *J. Geophys. Res.*, 102: 17825-17841.
92. Observational Evidence Observational Evidence from Supernovae for an Accelerating Universe and a Cosmological Constant, *Astronomical Journal* 116 (3): 1009-1038.
93. Oort, Jan H. (1932). The force exerted by the stellar system in the direction perpendicular to the galactic plane and some related problems, *Bulletin of the Astronomical Institutes of the Netherlands,* 6: 249-287.
94. Pejić, T. & Tkalčić, H. (2016). Toward attenuation tomography of the uppermost inner core from PKP waves, *Geophys Res Abstracts,* 18: EGU 2016-1605.
95. Penzias, A. A., Wilson, R. W. (1965). A Measurement of Excess Antenna Temperature at 4080 MHz, *Astrophysical Journal, 1*42: 419-421.
96. Perlmutter, S., Aldering, G., et al. (1999). Measurements of Omega and Lambda from 42 High-Redshift Supernovae, *The Astrophysical Journal,* 517 (2): 565-586.
97. Perrin, F. (2018). Discover Oklo, the world's only known natural nuclear reactor two billion years old, *Bulletin of International Atomic Energy Agency*, 59 (2): 26–27.
98. Peterson, J., Butler, H. M., Holcomb, L. G. & Hutt, C. R. (1976). Seismic Research Observatorium, *Bull. Seism. Soc. Am*. 66: 2049-2068.
99. Qamar, A. (1973). Revised velocities in the Earth's core, (Bulletin) *Seismol. Soc. Am*., 63: 1073- 1105.
100. Ramsey, W. H. (1948). On the constitution of terrestrial planets, *Mon. Not. Roy. Astron. Soc.*, 108: 406-413.
101. Rial, J. A. & Cormier, V. F. (1980). Seismic waves at the Epicenter's antipodes, *J. Geophys. Res.*, 91: 10203-10228.
102. Riess Adam G., et al. (1998). (High-z Supernova Search Team). (1998).
103. Ringwood, A. E. (1984). The Earth's Core: its composition, formation and bearing upon the origin of the Earth, *Proc. R. Soc.* A, 395: 1-46.
104. Rizo, H., et al. (2019). 182 W evidence for core-mantle interaction in the source of mantle plumes, *Geochem. Perspect. Lett*., 11, 6–11. https://doi.org/10.1016/j.geoperspect.2019.09.010.
105. Rodgers, A. & Wahr, J. (1993). Inference of core-mantle boundary topography from ISC PcP and PKP travel times, *Geophys. J. Int.* 115: 991-1011. doi: 10.1016/j.geojint.2011.09.010.
106. Rudnick, L., Brown, S. & Liliya, R. W. (2007). Extragalactic Radio Sources and the WMAP Cold Spot, *The Astrophysical Journal,* 671(1): 40.
107. Ruff, L. & Anderson, D. L. (1980). Core Formation, Evolution, and Convection: A Geophysical Model, *Phys. Earth Planet. Inter.*, 21**:** 181-201.
108. Scherk, J., Schwarz, J. H (1975). Dual field theory of quarks and gluons, *Phys. Lett.*, 57(B): 463-466.
109. Shearer, P. & Masters, G. (1990). The density and shear velocity contrast at the inner core boundary, *Geophysics. J. Int*., 102: 491-498.
110. Shimizu, H., Poirier J. P. & Le Mouël, J. L. (2005). On crystallization at the inner core boundary, *Phys. Earth Planet. Inter*. 151: 37-51.
111. Siegfried, T. (1999). Hidden Space Dimensions May Permit Parallel Universes and Explain Cosmic Mysteries, *The Dallas Morning News*, July 5, 1999.
112. Singh, S. C., Taylor, M. A. J., Montagner, J. P. (2000). On the presence of liquid in Earth's inner core, *Science*, 287: 2471-2474.
113. Siraj, Amir; Chyba, Christopher F.; Tremaine, Scott. (2025). "Orbit of a Possible Planet X". *The Astrophysical Journal*. 10 January 2025, 978 (2): 139.
114. Soldati, G., Boschi, L., Mora, S. D., Forte, A. M. (2014). Tomography of core-mantle boundary and lowermost mantle coupled by geodynamics: joint models of shear and compressional velocity, *Annals of Geophysics,* 6: 57, https://doi.org/10.1016/j.ag.2016.09.010.
115. Soldati, G., Koelemeijer, P., Boschi, L. & Deuss, A. (2013). Constraints on core-mantle boundary topography

from normal mode splitting, *Geochem. Geophys. Geosyst*. 14.

116. Song, X. & Helmberger, D. V. (1995). A P wave velocity model of earth's core, *J. Geophys. Res.*, 100 (B7): 9817-9830.
117. Souriau, A. & Souriau, M. (1989). Ellipticity and density at the inner core boundary from subcritical PKiKP and PcP data, *Geophys. J. Int.*, 98: 39-54.
118. Souriau, A., Poupinet, G. (1991). The velocity profile at the base of the liquid core from PKP (BC + Cdiff) data: An argument in favor of radial inhomogeneity, *Geophys. Res. Lett.*, 18: 2023-2026.
119. Spergel, D. N., et al. (2003). First Year Wilkinson Microwave Anisotropy Probe (WMAP) Observations: Determination of Cosmological Parameters. The Astrophysical Journal Supplement Series, 148(1): 192, Table 10. Basic and Derived Cosmological Parameters: Running Spectral Index Model.
120. Spergel, D. N., et al. (2007). Three-Year Wilkinson Microwave Anisotropy Probe (WMAP) Observations: Implications for Cosmology, *The Astrophysical Journal Supplement Series*, 170(2): 380, Table 2. Power-Law CDM Model Parameters and 68% Confidence Intervals, 3 Year + All-Income Mean.
121. Stokes, G. M. & Michalsky, J. J. (1979). Cygnus X-1, *Mercury* 8: 60.
122. Stsrobinskii, A. A. & Zel'dovich, Z. B. (1988). Quantum Effects in Cosmology. *Nature*, 331: 25.
123. Sumita, I. & Olson, P. (1999). A laboratory model for convection in Earth's core driven by a thermally heterogeneous mantle, *Science*, 286: 1547-1549. https://doi.org/10.1016/j.science.2012.09.010.
124. Sumita, I., Olson, P. (2002). Rotating thermal convection experiments in a hemispherical shell with heterogeneous boundary heat flux: implications for the Earth's core. *J. Geophys. Res.*, 107: 2169. doi: 10.1016/j.jgeo.2016.09.016.
125. Susskind, Leonard. (2006). Father of String Theory Muses on the Megaverse. *The New York Academy of Science Publications*, April 14, 2006.
126. Sze, E.K.M., van der Hilst, R. D. (2003). Core Mantle Boundary Topography from Short Period PcP, PKP and PKKP data, *Phys. Earth Planet. Int.*, 135: 27-46.
127. Van Schmus, W. R. (1995). Natural Radioactivity of the Crust and Mantle, *Global Earth Physics: A Handbook of Physical Constants*, 283-291.
128. Walker, R. J., Morgan, J. W. & Horan, M. F. (1995). Osmium-187 in some plumes: Evidence for core-mantle interaction? *Science*, 269, 819–822. https://doi.org/10.1016/j.science.1995.08.022.
129. Waszek, L. & Deuss, A. (2015a). Observations of Exotic Inner Core Waves, *Geophys. J. Int.*, 200 (3): 1636-1650.
130. Waszek, L. & Deuss, A. (2015b). Anomalously Strong Observations of *PKiKP/PcP* Amplitude Ratios on a Global Scale, *J. Geophys. Res. Solid Earth*, 120.
131. Woit, P. (2013). The "Dark Flow" & Existence of Other Universes –New Claims of Hard Evidence, *New Scientis*, June 3, 2013.
132. Woodhouse, J. H. & Dziewonski, A. M. (1989). Seismic modeling of the Earth's large-scale three-dimensional structure, *Phil. Trans. R. Soc. Lond,* A 328, 291-308.
133. Yoshida, M. (2008). Core-mantle boundary topography estimated from numerical simulations of instantaneous flow, *Geochemistry, Geophysics, and Geophysics,* 9 (7).
134. Young, C. J. & Lay, T. (1987). The core-mantle boundary, *Ann. Rev. Earth Planet. Sci*., 15: 25-46.
135. Yu, W., Wen, L., Niu, F. (2005). Seismic velocity structure in the Earth's outer core, *J. Geophys. Res.*, 110: B02302.
136. Zou, Z., Koper, K. D., Cormier, V. F. (2008). The structure of the base of the outer core inferred from seismic waves diffracted around the inner core, *J. Geophys. Res.*, 113, B05314. https://doi.org/10.1016/j.jgr.2013.01.013.
137. Zwicky, F. (1937). On the Masses of Nebulae and of Clusters of Nebulae, *Astrophysical Journal*, 86: 217.